

Long range dark matter self-interactions and plasma instabilities

Robert Lasenby

Stanford Institute for Theoretical Physics, Stanford University, Stanford, CA 94305, USA

E-mail: rlasenby@stanford.edu

ABSTRACT: So far, the observed effects of dark matter are compatible with it having purely gravitational interactions. However, in many models, dark matter has additional interactions with itself, with the Standard Model, and/or with additional hidden sector states. In this paper, we discuss models in which dark matter interacts through a light vector mediator, giving rise to a long-ranged force between dark matter particles. Coherent scattering effects through this force can lead to the exponential growth of small perturbations, in analogy to electromagnetic plasma instabilities. These instabilities can be significant at couplings many orders of magnitude below those for which the usual particle-by-particle constraints on dark matter self-interactions apply. While this possibility has been noted in the literature, we provide the first systematic study of such instabilities, including the case where the mediator has finite mass. The latter is relevant for models of kinetically mixed ‘dark photon’ mediators, which represent an important target for proposed dark matter detection experiments. Our analyses are of the growth of small perturbations, so do not immediately provide observational constraints on dark matter models — however, they do motivate further study of large regions of parameter space.

Contents

| | | |
|----------|---|-----------|
| 1 | Introduction | 1 |
| 1.1 | Parametrics of plasma instabilities | 3 |
| 1.2 | Previous literature | 5 |
| 2 | Plasma instabilities | 6 |
| 2.1 | Instabilities in a uniform plasma | 6 |
| 2.2 | Electrostatic instabilities | 9 |
| 2.2.1 | Beam-plasma | 13 |
| 2.3 | Magnetic instabilities | 16 |
| 3 | Astrophysical systems | 18 |
| 3.1 | Observational consequences | 23 |
| 4 | Millicharged DM | 24 |
| 5 | Kinetically mixed mediator | 25 |
| 5.1 | Existing constraints | 26 |
| 5.2 | Plasma instabilities | 28 |
| 5.3 | Dark matter parameter space | 29 |
| 6 | Light bosonic DM | 31 |
| 7 | Conclusions | 33 |
| A | Maxwellian velocity distribution | 35 |
| B | Penrose stability criteria | 35 |

1 Introduction

There is overwhelming evidence that most of the universe’s matter density consists of states other than Standard Model (SM) particles. All of the evidence for this ‘dark matter’ (DM) comes from its gravitational effects on astrophysical objects, and current observations are compatible with gravity being the only way in which DM interacts, either with itself or with the SM. Nevertheless, in many models of theoretical and experimental interest, DM must have additional interactions. Examples include WIMP DM, whose interactions with the SM radiation bath are responsible for its cosmological abundance, and the QCD axion, which has a self-interaction potential arising from its coupling to QCD. In all of these cases,

DM interactions must be weak enough that its behaviour looks effectively non-collisional, on the galactic scales that we have observational data for.

In this paper, we will focus mainly on DM self-interactions. For models such as WIMP DM, the DM number density is low (the occupation number of particle modes in halos is $\ll 1$), and the interactions between DM particles are short-ranged compared to the interparticle distance. Consequently, scattering is dominated by two-particle events. The standard DM self-interaction bounds from systems such as the Bullet Cluster [1] are based on this scenario. For DM masses in the GeV range, these constrain the interaction cross-section at around the barn level [2], comparable to SM nuclear cross-sections. The usual WIMP dark matter candidates, which have significantly heavier masses and weak-scale interactions, are safe from such constraints.

In other models, DM self-interactions can be long-ranged. For the simplest examples, DM particles interact with a light mediator, whose mass is small compared to the inverse spacing between DM particles. Quantitatively,

$$n_{\text{DM}} = \frac{\rho_{\text{DM}}}{m_{\text{DM}}} \simeq (4 \times 10^{-4} \text{ eV})^3 \frac{\text{MeV}}{m_{\text{DM}}} \frac{\rho_{\text{DM}}}{10 \text{ GeV cm}^{-3}} \quad (1.1)$$

$$\simeq (0.5 \text{ mm})^{-3} \frac{\text{MeV}}{m_{\text{DM}}} \frac{\rho_{\text{DM}}}{10 \text{ GeV cm}^{-3}} \quad (1.2)$$

where 10 GeV cm^{-3} corresponds to the highest DM halo density for which we have good evidence (unless otherwise noted, we use natural units with $\hbar = c = 1$). If the mass m of the mediating particle satisfies $m \ll n_{\text{DM}}^{1/3}$, then DM particles can interact coherently with many others. These interactions are coherently enhanced, and can have much larger rates than standard $2 \rightarrow 2$ scatterings. Of course, they are also softer (transferring less energy and momentum), and their behaviour may be much more complicated. This scenario can be contrasted to the ‘long-range’ mediators that are used to implement velocity-dependent DM scattering (e.g. [3]) — in that case, we only need the mediator mass to be $\lesssim q$, where q is the typical momentum transfer in a $2 \rightarrow 2$ collision. For example, in a typical galactic halo, $q \sim 10^{-3} m_{\text{DM}}$.

There are various theoretical motivations for long-range hidden sector mediators. Examples include hidden sector counterparts of the photon (e.g. in scenarios such as Twin Higgs models [4, 5]), light scalars [6–10], or other forms of ‘modified gravity’ (e.g. [11]). Such models are also important as an experimental target for low-threshold direct detection experiments, as we discuss in Section 5.

The effects of coherent, many-many scattering processes will depend on the form of the DM-mediator interaction. For a spin-0 mediator ϕ , the simplest kinds of interactions (e.g. $\phi \bar{\chi} \chi$, for a DM fermion χ) will be universally attractive for a given particle species, i.e. χ particles and antiparticles all interact attractively. This is basically the scenario of ‘modified gravity’ in the DM sector, a number of models for which have been explored in the literature (e.g. [6–10]).

For a spin-1 mediator A_μ , the simplest forms of interactions, e.g. $A_\mu \bar{\chi} \gamma^\mu \chi$, are analogous to electromagnetism.¹ If the cosmological DM abundance is net neutral, with equal

¹Higher-dimensional couplings, or couplings to a non-conserved current, result in a non-renormalisable

numbers of positive and negative charges, then (in the absence of large-scale charge separation) there will not be coherent forces between bulk matter, unlike in ‘modified gravity’ scenarios. In cosmological terms, inflation naturally sets any charge asymmetry to zero, and any processes regenerating it later must break the associated $U(1)$. However, even for DM that is bulk neutral, there can still be significant ‘plasma effects’, driven by coherent many-many scatterings. Analogous coherent EM effects are extremely important in SM astrophysics, driving processes such as shocks, jets and other collective phenomena [12].

This paper will investigate scenarios in which DM interacts through a light vector mediator. As we will see, coherent effects can be important even with very small DM-mediator couplings; in some cases, many orders of magnitude smaller than those constrained by $2 \rightarrow 2$ scattering processes. This raises the possibility of much stronger constraints on such DM models, or equivalently, observational signatures at much weaker couplings. While the possibility of these effects has been noted in the literature [13], we provide a systematic analysis. In addition to considering massless vectors, we also consider mediators with a small but finite mass, as well as those with couplings to SM matter as well as to DM. These more complicated models are important phenomenological targets, in particular for proposed experiments aiming to detect light DM candidates.

1.1 Parametrics of plasma instabilities

Despite the simple underlying physics, plasma dynamics — the behaviour of charged matter interacting via a light vector mediator — is an immensely complicated subject. The great variety of different behaviours of SM matter in astrophysical systems, much of which is driven by the combination of EM and gravity, illustrates this richness [12]. Accordingly, this paper will not attempt to categorise all of the different kinds of behaviour that could occur in the presence of long-range DM interactions. Instead, we will focus on identifying the smallest couplings for which coherent effects would be important in astrophysical settings. This should help guide future investigations of such models, and identify regions of parameter space where we might expect deviations from collisionless behaviour.

In many circumstances, the first effects to become important, as we increase the coupling from zero, are exponentially-growing instabilities. For a non-relativistic plasma, the fastest-growing of these instabilities are ‘electrostatic’ ones, in which small charge separation perturbations grow, by extracting kinetic energy from a non-Maxwellian velocity distribution [14]. The simplest case is a ‘two-stream’ instability, in which two uniform ‘streams’ of plasma pass through each other at high velocity (relative to their individual velocity dispersions). Perturbations, in the form of longitudinal charge-density waves, are exponentially amplified, with growth rate $\sim \omega_p$, where $\omega_p^2 = q^2 n / m_q$ is the ‘plasma frequency’, q the charge of individual particles, m_q their mass, and n their number density [15].

Taking our ‘plasma’ to be composed of dark matter particles, interacting through a hidden-sector vector mediator, this two-stream scenario approximates a collision between the DM halos of two galaxy clusters, such as the Bullet Cluster [1, 16]. In that system,

theory that must be completed above some energy scale.

the central densities of the colliding clusters' DM halos are modelled to be $\gtrsim 0.1 \text{ GeV cm}^{-3}$ (see Section 3). This DM density gives a plasma frequency of

$$\omega_p = \sqrt{\frac{g^2 \rho_\chi}{m_\chi^2}} \simeq 4 \times 10^{-7} \text{ yr}^{-1} \sqrt{\frac{\rho_\chi}{0.1 \text{ GeV cm}^{-3}}} \frac{\text{GeV}}{m_\chi} \frac{g}{10^{-17}} \quad (1.3)$$

where m_χ is the DM mass, ρ_χ is the DM density, and g is the DM-mediator coupling. The scale radius of the DM halos is $\sim 100 \text{ kpc}$, and their relative velocity is $\sim 3000 \text{ km s}^{-1}$, giving a crossing time of $\sim 100 \text{ kpc}/(3000 \text{ km s}^{-1}) \sim 3 \times 10^7 \text{ yr}$. Comparing ω_p^{-1} to this crossing time, we see that the exponential growth of perturbations could occur even for $g \lll 1$. For comparison, constraints from $2 \rightarrow 2$ particle scattering give $g \lesssim 4 \times 10^{-3} (m_\chi / \text{GeV})^{3/4}$ (see Section 5.1).

This estimate shows that coherent effects may become important at DM-mediator couplings orders of magnitude smaller than those at which $2 \rightarrow 2$ scatterings have significant effects. A natural question is what the observational consequences of coherent effects might be, and whether they can give observational constraints or potential signatures for such models. As discussed at the start of this section, plasma behaviour can be extremely complicated, and we will not try to answer this question in generality. However, in Section 3.1, we discuss some of the first observational signatures that may arise as we increase the DM-mediator coupling from zero. For cluster collisions, such as the Bullet Cluster, we might expect DM-DM momentum transfer to alter the post-collision DM density profile, leaving it more similar to that of the SM gas than the (effectively collisionless) stars. For DM subhalos moving within larger halos (e.g. dwarf galaxies in the Milky Way halo), potential effects include a drag force on the subhalo, modifying its orbit, or heating, resulting in its expansion / evaporation. Developing a proper understanding of these potential signatures is left to future work.

In the remainder of this paper, we analyse the growth of small perturbations more generally and quantitatively. In particular:

- We review the linear theory of instabilities in a homogeneous plasma (Section 2). Standard electromagnetic theory can be applied directly to the case of DM interacting via a massless hidden-sector mediator, simply by modifying the charges and masses of the particles.
- We extend this theory to the case of a massive vector mediator (Section 2). We find that mediator masses $m \gtrsim \omega_p / v_{\text{th}}$ suppress the growth of perturbations, where v_{th} is the velocity dispersion of the plasma. For velocity distributions without multiple peaks (such as an anisotropic Maxwellian distribution), only magnetic instabilities exist, and these are suppressed for $m \gtrsim \mathcal{O}(\omega_p)$.
- We identify regions in the m_χ, m_A, g_χ parameter space (where m_χ is the DM mass, m_A is the mediator mass, and g_χ is the DM-mediator coupling) where we expect small perturbations to grow in astrophysical systems (Section 3). At small m_A , the potential constraints on g_χ are many orders of magnitude stronger than those from

$2 \rightarrow 2$ scattering (this is illustrated in Figures 6 and 7). Observational signatures that may lead to such constraints are discussed in Section 3.1. We also comment on the potential for improved constraints when the DM is so light ($m \lesssim \text{eV}$) that it has occupation number $\gg 1$ in halos (Section 6).

- We study models in which DM interacts non-gravitationally with both itself and with SM matter, through a ‘dark photon’ vector mediator that kinetically mixes with the SM photon (Section 5). This is one of the simplest such possibilities, and represents an important target for low-threshold direct detection experiments. In large parts of the theoretically and experimentally interesting parameter space, we find that DM-DM plasma instabilities would be expected to grow exponentially in astrophysical systems (Figure 10). This motivates further investigations to determine whether such models are astrophysically viable. We also discuss why such effects may not be as important for the case of millicharged DM (Section 4).

1.2 Previous literature

To our knowledge, the first paper to raise the possibility of strong constraints from coherent DM-DM scattering was [13]. This considered DM interacting through a massless, purely dark-sector vector mediator, and focussed mainly on the constraints and signatures arising from $2 \rightarrow 2$ scattering. However, it also commented on the possibility of a magnetic Weibel instability (see section 2.3), and noted that such phenomena may provide significantly stronger constraints than $2 \rightarrow 2$ scattering, while leaving further investigations to future work.

In unpublished work, [17] identified the electrostatic two-stream instability as being faster-growing than the Weibel instability (again, for the case of a massless hidden-sector mediator), and estimated the parameter space where constraints from Bullet Cluster type systems might exist. In addition, they conducted preliminary simulations of such cluster collision scenarios.

[18] also identified the electrostatic two-stream instability as the fastest-growing one, and argued that since this instability would make DM effectively collisional, ‘models where all of DM is charged are ruled out by observations of cluster collisions unless the charge is extremely small’ (though they did not attempt to quantify this). Their main focus was a scenario in only a sub-component of DM is self-interacting through a massless hidden-sector mediator. In [19], cluster collisions with such a subcomponent were simulated, assuming that it behaves like a fluid with some effective viscosity.

Coherent interactions involving DM have been investigated extensively in the context of millicharged DM, where DM is taken to have a (very small) charge under Standard Model EM. As discussed in Section 4, the most important interactions are generally ‘one-many’, with individual DM particles scattering off the large-scale EM fields created by SM charges and currents. While some of this literature (e.g. [20]) claims that similar bounds apply to models with massive mediators, such as kinetically mixed dark photons, this is only true when the mediator mass is extremely small (see Section 5). There have also been investigations of whether ‘many-many’ collective instabilities can be important for

millicharged DM [21], but further work would be needed to establish whether this could occur for couplings not excluded by other effects.

DM coupled to a light vector mediator is considered in many other papers (e.g. [22–25]), but in most cases, they do not consider plasma effects (or if they do, only insofar as they affect Coulomb scattering through Debye screening — see Section 5.1). [26] does consider plasma effects in a model with a massive hidden-sector mediator, but focusses on the properties of the DM plasma near Earth (in the context of direct detection experiments), rather than on systems such as cluster collisions.

2 Plasma instabilities

In this section, we will discuss the linear theory of plasma instabilities. Astrophysically, the DM distributions that arise from collisionless evolution will often be very far from thermal equilibrium (for example, the basically-bimodal velocity distributions in cluster collisions). Given strong enough interactions, such a distribution will relax towards equilibrium.² For some distributions, the initial stages of this relaxation are driven by exponentially-growing instabilities, which grow by converting particle kinetic energy into field energy.

2.1 Instabilities in a uniform plasma

We will begin by considering perturbations of a spatially uniform plasma, in a freely falling frame, with no large-scale currents or charge separation in the initial state. In real astrophysical systems, spatial inhomogeneities and gravitational forces are, of course, often important. However, if the spatial scale of a perturbation is small, these approximations can be good, and as we will see, the spatial scales associated with instabilities are often small enough. If the initial state does not feature large-scale currents or charge separation, then (for large enough DM number densities that particle number effects are not important), these must have arisen through interactions becoming important at earlier times. Consequently, to analyse the earliest point at which large-scale vector fields arise, we can start from approximately zero-field conditions.

In terms of the distribution functions $f_s(v, x, t) = \frac{dN_s}{d^3v d^3x}$ of the particle species s in the plasma, conservation of phase space density along particle trajectories requires that

$$\partial_t f_s + v \cdot \partial_x f_s + a_s \cdot \partial_v f_s = 0 \quad (2.1)$$

where $a_s = \frac{dv}{dt} = \frac{q_s}{m_s}(E + v \times B)$ is the acceleration due to the Lorentz force, with q_s and m_s the charge and mass of species s . The charge density, $\rho = \sum_s q_s \int d^3v f_s$, and the current density, $J = \sum_s q_s \int d^3v v f_s$, give the source term J^ν in the Proca equations $(\partial_\mu \partial^\mu - m^2)A^\nu = J^\nu$ (where m is the mass of the vector mediator, and we use the $+- --$ signature). Together, these equations determine the evolution of the plasma distribution function.

²When gravitational interactions are important, there is generally no equilibrium state for a particle system; entropy can always be increased by a subset of the particles becoming more tightly bound [27, 28]. However, as we will discuss, the plasma instabilities that we are interested in will generally be important on scales well below those where gravity is important.

For a particular configuration of charged particles, the distribution function will be a set of delta-functions corresponding to the positions and momenta of these particles, and solving the above equations will correspond to solving the interacting N -body system. To simplify things, we need to perform some kind of averaging. One approach is to coarse-grain in position and velocity space, so that there are many charged particles in each phase-space ‘bin’ — another is to track the evolution of an ensemble-averaged distribution function, where we average over e.g. different possible starting configurations of the particles [29]. In either case, for the averaged solution to be a good approximation to the particular solution, we need the particles in the latter to be sufficiently dense in phase space. We will return to this condition in Section 2.2.

Since E and B , and consequently a_s , depend on the particle trajectories, the $a_s \cdot \partial_v f_s$ term in equation 2.1 cannot simply be replaced by $\bar{a}_s \cdot \partial_v \bar{f}$, where the bar indicates averaging. In general, correlations need to be taken into account. However, the most important correlations generally arise from close encounters between particles. In situations where collective effects dominate, and individual collisions are unimportant, we can use the ‘collisionless Boltzmann equation’ (also referred to as the Vlasov equation) [29],

$$\partial_t \bar{f}_s + v \cdot \partial_x \bar{f}_s + \bar{a} \cdot \partial_v \bar{f}_s = 0 \quad (2.2)$$

(in the rest of the paper, we will usually drop the bars). Since a typical DM particle can only undergo $\mathcal{O}(1)$ hard collisions during the lifetime of the universe, without affecting observables such as galactic halo shapes (see Section 5.1), the collisionless Boltzmann equation will often be a good approximation, in parameter space which is not already constrained by analyses of $2 \rightarrow 2$ collisions.

If our unperturbed state is a spatially uniform distribution function f_s , with no vector field background, then the linear-order equations for a small perturbation $\delta f_s, A_\mu$ are

$$(\partial_t + v \cdot \partial_x) \delta f_s = -a(A_\mu) \cdot \partial_v f_s \quad , \quad (\partial_\mu \partial^\mu - m^2) A^\nu = \sum_s q_s \int d^3 v v^\nu \delta f_s \quad (2.3)$$

where $v^\nu = \gamma(1, v_i)$, with $\gamma = 1/\sqrt{1-v^2}$. We will work with non-relativistic velocity distributions, so will take $\gamma \simeq 1$. If we decompose the perturbations into Fourier modes, so $\delta f_s(t, x) = \delta f_s e^{-i(\omega t - k \cdot x)}$ etc, then we can express δf_s in terms of A_μ , giving a linear equation for A_μ :

$$(\omega^2 - k^2 - m^2) A^\nu = -i \sum_s q_s \int d^3 v v^\nu \frac{a(A_\mu) \cdot \partial_v f}{\omega - k \cdot v} \equiv \Pi^{\nu\mu}(\omega, k) A_\mu \quad (2.4)$$

where $\Pi^{\nu\mu}$ is the leading order response function (the ‘self-energy’, in the language of thermal field theory [30]). For a given k , there will be some particular ω for which this equation can be satisfied. These (k, ω) pairs give the dispersion relation for perturbations.

To take the simplest possible example, a cold, uniform plasma has $f_s = n_s \delta^3(v)$. We can evaluate equation 2.4 via integration by parts; if we assume that f decays fast enough at large velocities, then

$$\int d^3 v v_i \frac{((E + v \times B) \cdot \partial_v f)}{\omega - k \cdot v} = - \int d^3 v \frac{f}{\omega - k \cdot v} \left(E + v \times B + \frac{k \cdot (E + v \times B)}{\omega - k \cdot v} v \right)_i \quad (2.5)$$

So, for $f_s = n_s \delta^3(v)$, we have

$$(\omega^2 - k^2 - m^2)A_i = i \sum_s \frac{q_s^2 n_s}{m_s} \frac{E_i}{\omega} \quad (2.6)$$

Since $E = -\nabla\phi - \partial_t A$, and the Lorenz condition $\partial_\mu A^\mu = 0$ gives $\dot{\phi} + \nabla \cdot A = 0$, we have

$$(\omega^2 - k^2 - m^2)A_i = \left(\sum_s \omega_s^2 \right) \left(A_i - \frac{k_i k \cdot A}{\omega^2} \right) \quad (2.7)$$

where $\omega_s \equiv q_s^2 n_s / m_s$. For $m = 0$, this gives the usual dispersion relations for transverse and longitudinal excitations in a cold plasma [31]. Some more realistic examples, such as Maxwellian velocity distributions, can also be treated analytically (see appendix A).

One of the simplest examples that gives rise to exponentially growing perturbations is the ‘two-stream’ instability. If we consider a plasma consisting of positive and negatively charged species with the same mass (as we expect for symmetric DM models), this has $f_\pm = \frac{n_p}{2} (\delta^3(v - v_0) + \delta^3(v + v_0))$, corresponding to two cold ‘streams’ of plasma passing through each other. For longitudinal perturbations, i.e. those with $k \parallel A \parallel v_0$, we have

$$(\omega^2 - k^2 - m^2)A = (\omega^2 - k^2) \left(\frac{\omega_p^2}{(\omega - k \cdot v_0)^2} + \frac{\omega_p^2}{(\omega + k \cdot v_0)^2} \right) A \quad (2.8)$$

where $\omega_p = \sqrt{q^2 n_p / m}$ is the plasma frequency of each of the streams, with the charge of the two species being $\pm q$ and their mass being m . If we start with some localised perturbation at an initial time, we can decompose it into spatial Fourier modes with real k . Consequently, there are exponentially growing perturbations if there are solutions of the dispersion relation with $\text{Im} \omega > 0$ for real k . As we discuss in Section 2.2, such solutions exist for $m \leq \omega_p / v_0$, and the fastest growth rate is $\omega_i \simeq 0.5 \omega_s$ (attained for $k \simeq \omega_s / v_0$, and $m \ll k$).

We will discuss the physical understanding of this instability (and others) in detail below, but to start with, we can understand the parametrics of the growth rate simply by considering the energetics of the instability. The vector field’s energy density is $u_A = \frac{1}{2}(E^2 + B^2)$ (or larger for a massive mediator — see equation 2.12). The force exerted on a charged particle is $F = q(E + v \times B)$, so over a time δt , the magnitude of the change in the particle’s velocity is at most $\delta v \sim \frac{q \delta t}{m}(E + v \times B)$. For a collection of particles with charges q_i and velocities v_i , the rate of energy transfer from particle KE to field energy is $P = \dot{U}_A = -\sum_i q_i v_i \cdot E$.

If we suppose that our perturbation is growing exponentially, and we take δt to be the e -folding time, then we must have $\delta P \sim P$ and $\delta U_A \sim U_A$, so $\delta P \delta t \sim U_A$. For a perturbation where u_A is dominated by the electric field, such as the longitudinal modes in equation 2.8, we have $|\delta P \delta t| \lesssim \frac{q^2}{m} N (\delta t)^2 E^2$, where $N = nV$ is the number of particles in the volume V . Since $|\delta P \delta t|$ needs to be $\gtrsim u_A V \sim \frac{1}{2} E^2 V$ for the perturbation to grow, we have

$$\frac{q^2 n}{m} (\delta t)^2 \gtrsim 1 \quad \Rightarrow \quad \delta t \lesssim \left(\frac{q^2 n}{m} \right)^{-1/2} = \omega_p^{-1} \quad (2.9)$$

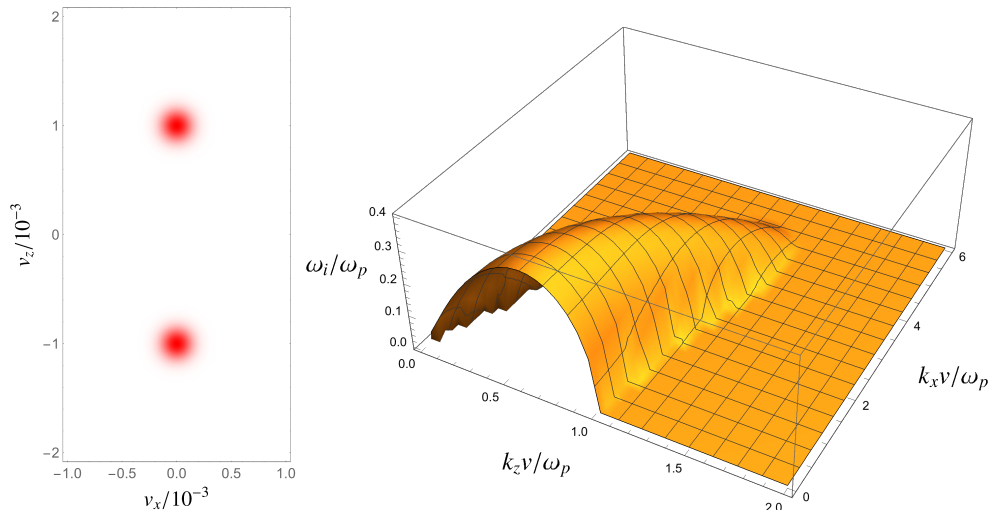


Figure 1. *Left panel:* velocity distribution for a ‘two-stream’ plasma background, in which two Maxwellian streams with velocity dispersion $\sigma = 10^{-4}c$ are counter-propagating, with a closing velocity $2 \times 10^{-3}c$ in the z direction. The shading indicates the phase space density at a given velocity. *Right panel:* fastest growth rate for a perturbation with wavevector k , on the plasma background illustrated in the left-hand panel. The height of the surface corresponds to the imaginary part of the mode’s frequency. The plasma is assumed to consist of positive and negatively charged species with the same mass, and having the same velocity distributions. We take $\omega_p^2 = q^2 n/m_q$, where n is the number density in each stream, $\pm q$ is the charge of each species, and m_q is their mass.

For a magnetic-field-dominated perturbation, the maximum growth rate is suppressed by some power of $v/c \ll 1$ (for a non-relativistic plasma).³ Consequently, the $\omega_i \sim \omega_p$ growth rate obtained from the two-stream instability is as fast as perturbations can grow, starting from a background without larger fields present (equivalently, it is the fastest rate at which the overall field energy can increase).

2.2 Electrostatic instabilities

As we will see, unstable modes in a non-relativistic plasma generally have $|k| \gg |\omega|$; parametrically, for the velocity distribution of the plasma to be significant, we need $|kv| \gtrsim \omega$. Consequently, instabilities in which the electric field perturbations are much larger than the magnetic field perturbations are dominantly electrostatic, with $|\phi| \gg |A|$ (since $B = \nabla \times A$ and $E = -\partial_t A - \nabla\phi$). In this case, we can simplify the Vlasov-Proca equations to a one-dimensional integral. Reinstating c for clarity, we have

$$(\omega^2 - c^2 k^2 - m^2 c^4)\phi = -i \sum_s \frac{q_s^2}{m} \int d^3v \frac{1}{\sqrt{1 - v^2/c^2}} \frac{((E + v \times B) \cdot \partial_v f_s)}{\omega - k \cdot v} \quad (2.10)$$

³If a Fourier mode of a perturbation has both E and B large, then its Poynting vector $S = E \times B$ is large, corresponding to a propagating photon. In our scenarios, this means that energy will be transported away from an initially localised perturbation, rather than the perturbation growing.

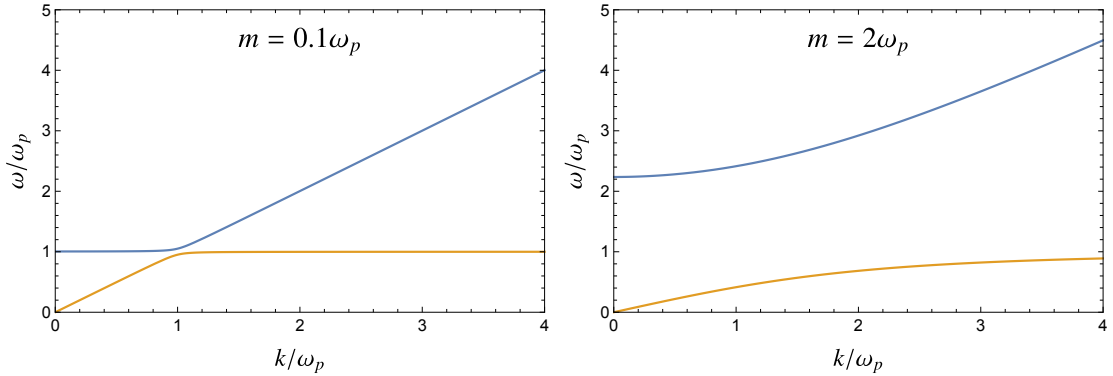


Figure 2. Dispersion relation for longitudinal oscillations in a cold, uniform plasma, with a massive mediator. In the left-hand panel, the mediator mass is $m = 0.1\omega_p$. Longitudinal plasmons, which for a massive mediator have $\omega = \omega_p$, are mostly unaffected (apart from a small avoided crossing). At small ω , there is also the $\phi \simeq \text{const}$ Goldstone mode (which would be pure-gauge for a massless mediator), and at high ω , there are relativistic ϕ excitations. In the right-hand panel, we have $m = 2\omega_p$. Here, longitudinal plasmons are strongly affected for $k \lesssim m$, linking with the Goldstone dispersion relation at smaller k . At higher ω , the dispersion relation is approximately that for a free massive particle.

so taking $E \simeq -ik\phi$,

$$(c^2k^2 + c^4m^2)\phi \simeq c^2\phi \sum_s \frac{q_s^2}{m} \int d^3v \frac{k \cdot \partial_v f_s}{\omega - k \cdot v} \quad (2.11)$$

which gives us a scalar equation for the dispersion relation. For purely longitudinal perturbations, the full Vlasov equation has this form (since there can be no magnetic fields), so the behaviour of electrostatic perturbations with a particular wavevector k is equivalent to longitudinal perturbations with the appropriate projected velocity distribution (see appendix B).

For a massless mediator, longitudinal perturbations have been extensively analysed in the plasma theory literature [15]. In the symmetric, two-stream scenario, a basic physical picture of the instability can be obtained (following [15]) by considering the longitudinal oscillations of each of the streams individually. For a stream with velocity v in the lab frame, oscillations with $\omega = \omega_p$ in the stream's rest frame have $\omega = k \cdot v \pm \omega_p$ in the lab frame⁴, and the 'slow' oscillation (with smaller frequency) has less kinetic energy than the unperturbed beam, $\Delta\text{KE} < 0$. If we take k such that $|k \cdot v| = \omega_p$, then the slow oscillations for both streams are stationary in the lab frame. If the two oscillations are in phase, they reinforce each other, extracting KE from the streams to increase the E field energy, and giving rise to an instability.

⁴In the case of symmetric DM, each stream will be composed of equal numbers of positive and negative charges, with both species having the same velocity distribution. If each has number density n_{\pm} then the plasma frequency for the stream is $\omega_p^2 = 2q^2n_{\pm}/m$. In the case of an SM plasma, we might instead have streams of electrons on top of a uniform, slowly-moving background of ions. The important quantity is simply the self-energy that the distribution function gives rise to, which determines the dispersion relation.

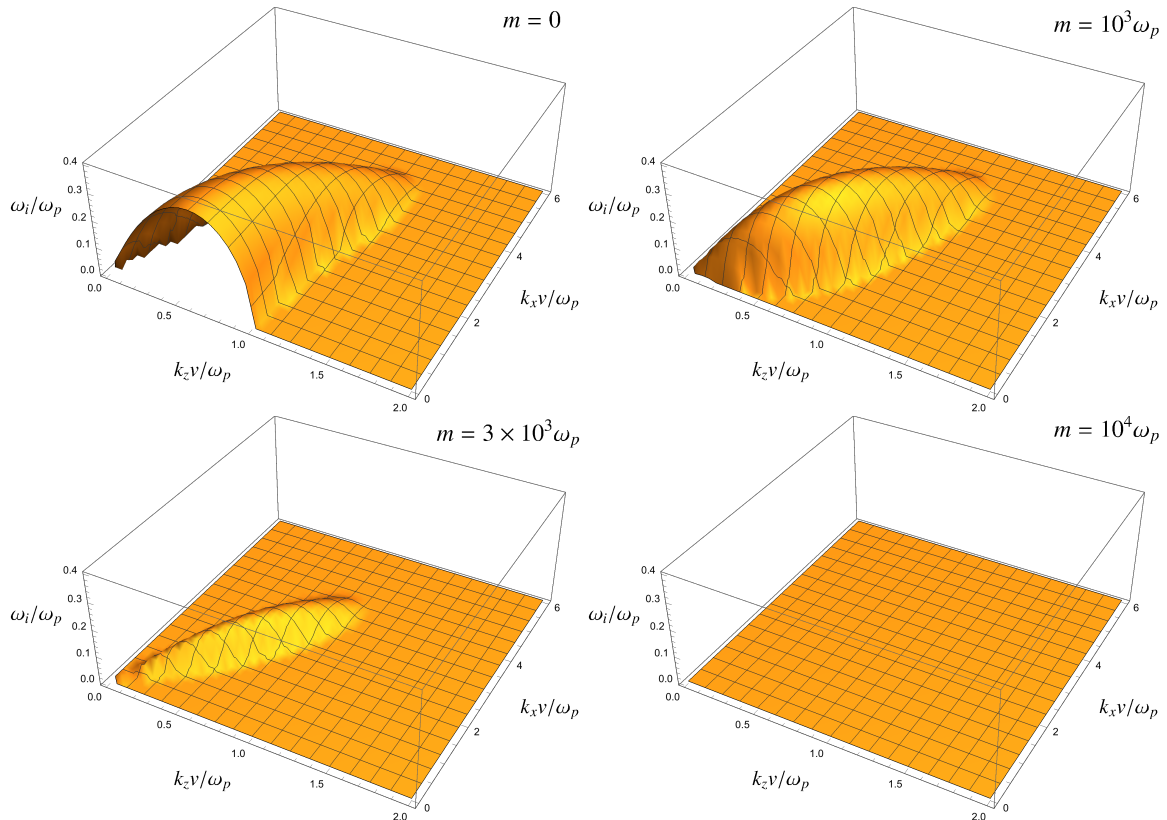


Figure 3. Fastest growth rate for a perturbation with wavevector k , on the plasma background illustrated in Figure 1, for a vector mediator of the indicated mass m . As this illustrates, longitudinal perturbations are suppressed for $m \gtrsim \omega_p/v_0 \sim 10^3 \omega_p$, while ‘oblique’ perturbations with significant k_x component exist up to $m \sim \omega_p/\sigma$ (see Section 2.2).

This is the relevant picture for $k \cdot v \simeq \omega_p$, where the peak instability rate is obtained. As Figure 1 shows, there are also growing perturbations with small k , for which $\omega_i \searrow 0$ as $k \searrow 0$. These can be thought of as arising from out-of-phase slow oscillations in each stream, such that (in the lab frame) the charge density perturbations almost cancel each other out.

A similar picture applies in the case of a massive mediator, with the difference that, for $m \gtrsim \omega_p$ and $k \lesssim m$, the dispersion relation for longitudinal oscillations in a stationary plasma is modified (see Figure 2). Consequently, the peak instability rate is modified for $m \gtrsim \omega_p/v$.

Even without solving equation 2.11 directly, we can determine whether an instability exists using the Penrose criteria [32] (see appendix B). If the two streams have Maxwellian (projected) velocity distributions, then for a massless mediator, an instability exists if $v_0 \gtrsim 1.3\sigma$, where σ is the velocity dispersion for each stream, and $2v_0$ is the closing velocity. For a massive mediator, even for well-separated stream velocity distributions (i.e. closing velocity \gg velocity dispersions), we need $m \lesssim 1.3\omega_p/v_0$ in order for an instability to exist.

Figure 1 illustrates a particular example of two Maxwellian streams moving through each other (with parameters roughly analogous to a cluster collision scenario), taking the closing velocity to be $2 \times 10^{-3}c$, and the velocity dispersion for each stream to be $\sigma_v = 10^{-4}c$. The height of the surface corresponds to the fastest instability rate for each k , which can be found from equation 2.11 (in fact, the figure uses the full Vlasov-Proca equation, rather than the longitudinal approximation, though the results are almost identical). As we go to more oblique k , the projected velocity distribution has a smaller closing velocity, so past the $v_p \simeq 1.3\sigma$ threshold, where $2v_p$ is the projected closing velocity, the instability does not exist (though magnetic instabilities may still be present, as we discuss in Section 2.3).

For a massive mediator, if the closing velocity is significantly greater than the velocity dispersions, then going to oblique k can be helpful, since it decreases v_p , and so increases ω_p/v_p . This is illustrated in Figure 3, which shows the effects on increasing m on the instability rate as a function of k . For $m \gtrsim \omega_p/\sigma$, the instability is suppressed entirely.

This behaviour matches what we would expect from basic energetic considerations. The energy density associated with the A field is

$$u_A = \frac{1}{2}(E^2 + B^2 + m^2((A^0)^2 + A^2)) \simeq \frac{1}{2}((\nabla\phi)^2 + m^2\phi^2) \quad (2.12)$$

where the second equality is for an electrostatic perturbation. Consequently, we expect the mediator mass to become significant when $m \gtrsim k$, as we observed above.

As mentioned in Section 2.1, for the collisionless Boltzmann equation to be a good approximation to the evolution of a particular plasma configuration, the particle density in phase space needs to be sufficiently high. If the largest wavenumber of interest is k , then having many particles per $\sim k^{-3}$ volume means that we have a sensible spatial coarse-graining. Within each k^{-3} , we ideally want enough particles to resolve the important features of the velocity distribution. For the two-stream instability, the relevant condition is $n_\chi \gg (\omega_\chi/\sigma)^3$. If we impose the $2 \rightarrow 2$ Coulomb scattering bound (equation 5.5), and also that $g \leq 1/(4\pi)$ (when m_χ is large enough that the Coulomb bound is ineffective), then

$$\frac{n_\chi}{(\omega_\chi/\sigma)^3} = \frac{\sigma^3 m_\chi^2}{\rho_\chi^{1/2} g^3} \gtrsim 10^{20} \left(\frac{\sigma}{10^3 \text{ km s}^{-1}} \right)^3 \left(\frac{0.1 \text{ GeV cm}^{-3}}{\rho_\chi} \right)^{1/2} \quad (2.13)$$

Consequently, the dark matter number density is always high enough that, in a spatially uniform plasma, there would be a good coarse-grained description. We discuss how well the approximation of spatial uniformity applies to astrophysical systems in Section 3.

The other way in which the collisionless Boltzmann equation can break down is if collisions are important. For hard collisions, the obvious estimate is that, if the collision rate for a particle is comparable to the growth time for the instability, then the instability will be suppressed. This can be confirmed by explicit calculations [15]. For Coulomb collisions, the rate of soft collisions is enhanced by a Coulomb logarithm factor (Section 5.1), but this alters things by a factor of $\mathcal{O}(10)$ at most [13, 24]. As we noted above, since only a few hard collisions per DM particle during the lifetime of universe are enough to significantly affect e.g. halo shapes [13, 24], neglecting collisions will usually be a good approximation for couplings that are not already excluded by $2 \rightarrow 2$ scattering calculations. As we will see

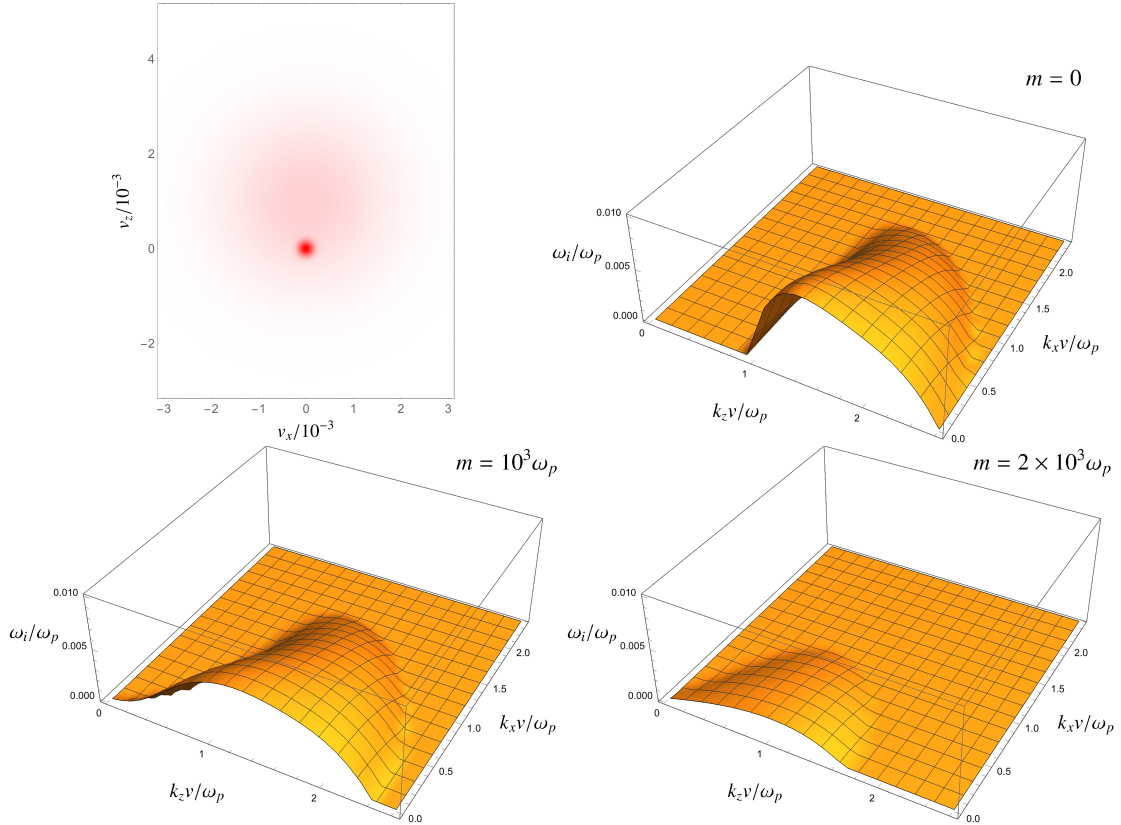


Figure 4. *Top-left panel:* velocity distribution for a ‘beam-plasma’ scenario, in which a dense ($\omega_p = 1$, in arbitrary units), low velocity dispersion ($\sigma_p = 10^{-4}c$) Maxwellian stream propagates through a more dilute ($\omega_p = 0.1$), high velocity dispersion ($\sigma = 10^{-3}c$) at relative velocity $v = 10^{-3}c$. *Other panels:* fastest growth rate for a perturbation with wavevector k , on the plasma background illustrated in the top-left panel, for a vector mediator with the masses m indicated. For $m \gtrsim 2.5 \times 10^3 \omega_p$, there are no unstable modes.

in Section 3, the couplings we are interested in are often many orders of magnitude below $2 \rightarrow 2$ exclusion limits. Consequently, even if regions of very high DM density exist, such as sharp central cusps in halos, collisions will usually be unimportant even there.

2.2.1 Beam-plasma

If we consider asymmetric streams, as illustrated in Figure 4, the behaviour of instabilities can be somewhat different. In the plasma literature, these are known as ‘beam-plasma’ instabilities, with the ‘beam’ being the less dense stream and the ‘plasma’ the more dense one [15]. For us, they can serve as a model for astrophysical situations such as a denser, lower-velocity-dispersion subhalo (the ‘plasma’) moving through a larger DM halo (the ‘beam’), as discussed in Section 3.

Setting up our problem (for a massless mediator, our calculations will follow those in [15]), we will take the denser stream to be at rest, with plasma frequency ω_p , and the less dense stream to have relative velocity v_0 , with plasma frequency ω_1 . If we ignore the

velocity dispersion of the streams, the dispersion relation for a massless mediator is

$$1 = \frac{\omega_p^2}{\omega^2} + \frac{\omega_1^2}{(\omega - kv_0)^2} \quad (2.14)$$

If we assume the density ratio is small, $R \equiv \omega_1^2/\omega_p^2 \ll 1$, then for $\omega \not\approx \omega_p$, we need $|\omega - kv_0|^2 \sim R$. Writing $\omega - kv_0 = \delta$, we have

$$\delta^2 = R \frac{\omega^2 \omega_p^2}{\omega^2 - \omega_p^2} \quad (2.15)$$

Consequently, for $\omega \gtrsim \omega_p$, the modes are stable, while for $\omega \lesssim \omega_p$, we have $\omega_i \sim \sqrt{R}ku$. The maximum instability rate is obtained for $\omega \simeq \omega_p$, for which

$$\delta^2 \simeq R \frac{\omega^2 \omega_p}{2\delta} \quad \Rightarrow \quad \delta^3 \simeq \frac{R}{2} \omega_p^3 \quad \Rightarrow \quad \delta \simeq e^{2\pi i n/3} \left(\frac{R}{2}\right)^{1/3} \omega_p \quad (2.16)$$

where n is an integer. Consequently, the maximum growth rate is $\omega_i \sim R^{1/3}\omega_p$.

Neglecting the velocity dispersions of the streams will be a good approximation if the phase velocity of the excitation is well outside the velocity distributions of both streams. In the plasma literature, this is referred to as the ‘cold-beam’ case. Since $\omega/k - v_0 = \delta/k$, this will be true if the fractional velocity dispersion of the beam is $\frac{\sigma}{v_0} \lesssim \max \frac{\delta}{kv_0} \sim R^{1/3}$, and the plasma velocity dispersion is $\ll v_0$.

The physical picture for the fastest-growing instability is that a longitudinal oscillation in the denser stream, which has frequency ω_p , interacts with a $\Delta KE < 0$ forced oscillation in the ‘beam’, extracting kinetic energy. For $kv_0 \lesssim \omega_p$, we have a similar picture as for the two-stream instability, with partially-cancelling perturbations in the beam and the plasma. As we take $R \rightarrow 1$, we move smoothly towards the two-stream case.

In many circumstances, the beam’s velocity dispersion will be large enough that the ‘cold-beam’ approximation does not hold. For example, in the subhalo case, the velocity dispersion of the larger halo is generally comparable to the orbital velocity of the subhalo through it, so $\sigma \sim v_0$. The behaviour in this ‘hot-beam’ scenario is rather different.

Since we need to take the beam’s velocity distribution into account, the dispersion relation for longitudinal oscillations becomes (again, for a massless mediator)

$$1 \simeq \frac{\omega_p^2}{\omega^2} + \frac{\omega_1^2}{k^2} \int dv \frac{f'(v)}{\omega/k - v} \quad (2.17)$$

(we will see that as long as the plasma’s velocity dispersion is $\ll u$, treating it as cold will not affect the most unstable modes). If we write $\omega/k = u_r + iu_i$, then we can write the integral over v as an integral over a contour slightly below the real axis, which for u_i sufficiently small is approximately

$$\int dv \frac{f'(v)}{v - (u_r + iu_i)} = \int_{-\infty - iu_i}^{\infty - iu_i} dv \frac{f'(v + iu_i)}{v - u_r} \simeq P \int_{-\infty}^{\infty} dv \frac{f'(v)}{v - u_r} + i\pi f'(u_r) \quad (2.18)$$

For the imaginary part of equation 2.17 to be zero, we need

$$-\frac{2\omega_p^2\omega_r\omega_i}{|\omega|^4} + \pi\frac{\omega_1^2}{k^2}f'(\omega_r/k) \simeq 0 \quad (2.19)$$

For $R \ll 1$, the real part of the RHS of equation 2.17 is dominated by the first term ω_p^2/ω^2 , so we need $\omega_r \simeq \omega_p$. Consequently,

$$\omega_i \simeq R\omega_p\frac{\pi}{2}\frac{\omega_p^2}{k^2}f'(\omega_r/k) \quad (2.20)$$

For a generic beam velocity distribution, with velocity dispersion $\sim \sigma$, the maximum value of $f'(u)$ is $\sim 1/\sigma^2$, so

$$\max \omega_i \sim R\omega_p\frac{u^2}{\sigma^2} \quad (2.21)$$

For this to be valid, we need $f'(u_r + iu_i) \simeq f'(u_r)$; for a simple beam velocity distribution such as a Gaussian, this requires $u_i \ll \sigma$. From equation 2.21, this holds for $R \ll \sigma^3/v_0^3$. This is simply the opposite of the cold-beam condition derived above, showing that the hot-beam and cold-beam regimes are complementary. The maximum instability rates also have the same parametric value at $R \sim \sigma^3/v_0^3$, consistent with this picture.

The different behaviour in the hot-beam regime corresponds to a somewhat different physical picture of the instability, compared to the cold-beam case. In particular, the approximation of the counter integral used above is very similar to the usual derivation of Landau damping [14, 29]. For the latter, the physical picture is that beam particles with velocities very slightly smaller the phase velocity ω/k of a plasma oscillation are accelerated by it, while those with velocities very slightly larger are slowed down. If the gradient of the velocity distribution is negative, then there are more slightly-slower particles than slightly-faster particles, and energy is on average transferred from the plasma oscillation to particle KE. If the gradient is *positive*, then the opposite occurs; energy is transferred from particle KE to the plasma oscillation, resulting in an instability. This ‘inverse Landau damping’ picture breaks down when the instability growth rate becomes too fast, so that ‘slightly-slower’ and ‘slightly-faster’ encompass too wide a range in the velocity distribution.

The top-right panel of Figure 4 shows the instability behaviour for an example velocity distribution with $R = 10$, and $\sigma = v$ (i.e. in the hot-beam regime). While the ω_r values of the unstable modes are not shown, these are close to ω_p . As the figure illustrates, we need $k \cdot v \gtrsim \omega_p$ for there to be an instability, corresponding to the phase velocity of the perturbation being in the increasing part of the v_z distribution.

For a massive mediator, the same basic physical picture applies, once the modified dispersion relation of longitudinal oscillations is taken into account. Equation 2.17 is modified to

$$1 + \frac{m^2}{k^2} \simeq \frac{\omega_p^2}{\omega^2} + \frac{\omega_1^2}{k^2} \int dv \frac{f'(v)}{\omega/k - v} \quad (2.22)$$

From the real part of this equation, we need to have $\omega \simeq \omega_p(1 + m^2/k^2)^{-1/2}$. This corresponds to the lower branch of the dispersion relation (for the dense plasma) in the right-hand panel of Figure 2, with the usual relation $\omega \simeq \omega_p$ being modified for $m \gtrsim k$.

Parametrically, we expect instabilities to be suppressed entirely for $m \gtrsim \frac{\omega_p}{\sigma_p}$. For longitudinal oscillations, we can confirm this using the Penrose criteria; from appendix B, instabilities exist for

$$m \lesssim \frac{\omega_p}{v_c} \sim \frac{\omega_p}{\text{few} \times \sigma_p} \quad (2.23)$$

where v_c is the point at which $f'_v = 0$, balanced between the falling f' from the plasma velocity distribution and the rising f' from the beam. The second equality applies if both the beam and plasma have Maxwellian velocity distributions. The basic physical picture is that, for given k , increasing m pushes ω_r smaller, until $u_r = \omega_r/k$ is no longer on the rising part of the velocity distribution (see Figure 12). This behaviour is illustrated in Figure 4, which shows the effects of increasing m on the instability rate as a function of k . Since the velocity distribution of the dense component is isotropic, and the dense component's velocity dispersion sets the largest k for an unstable mode, it does not help to go to oblique k .

2.3 Magnetic instabilities

The electrostatic instabilities discussed above relied on velocity distributions with sufficiently well-separated peaks. As well as these, there can also be ‘magnetic’ instabilities, in which the magnetic field energy dominates the electric field [33, 34]. In situations where both magnetic and electrostatic instabilities exist, the growth rate of the former is generally suppressed relative to the latter by $\sim v_s/c$, where v_s is the stream velocity. However, magnetic instabilities exist for a wider range of velocity distributions, including those which are very close to Maxwellian.

The simplest examples of magnetic instabilities can be seen in the (cold) two-stream velocity distribution [34]. If, instead of looking at $k \parallel v_0$ perturbations, we take $k \perp v_0$, then the response function is (taking the streams to be in the z direction, and $k \propto \hat{x}$)

$$\Pi A = \begin{pmatrix} (\omega^2 - k^2) \frac{\omega_p^2}{\omega^2} & 0 & 0 \\ 0 & \omega_p^2 & 0 \\ 0 & 0 & (\omega^2 + k^2 v_0^2) \frac{\omega_p^2}{\omega^2} \end{pmatrix} \begin{pmatrix} A_x \\ A_y \\ A_z \end{pmatrix} \quad (2.24)$$

For $A \perp \hat{z}$, we have the usual dispersion relations for plasma oscillations (as we would expect, since non-relativistic motion in the \hat{z} direction has not effect on those). For $A \parallel \hat{z}$, the dispersion relation becomes

$$\omega^2 - c^2 k^2 - c^4 m^2 = \omega_p^2 + k^2 v_0^2 \frac{\omega_p^2}{\omega^2} \quad (2.25)$$

(where we have reinstated c for clarity) which has solution

$$\omega^2 = \frac{1}{2} \left(\omega_p^2 + c^2 k^2 + c^4 m^2 \pm \sqrt{(\omega_p^2 + c^2 k^2 + c^4 m^2)^2 + 4\omega_p^2 k^2 v_0^2} \right) \quad (2.26)$$

Expanding in small v_0/c , we have a solution

$$\omega^2 \simeq \frac{-\omega_p^2 k^2 v_0^2}{\omega_p^2 + c^2 k^2 + c^4 m^2} \quad (2.27)$$

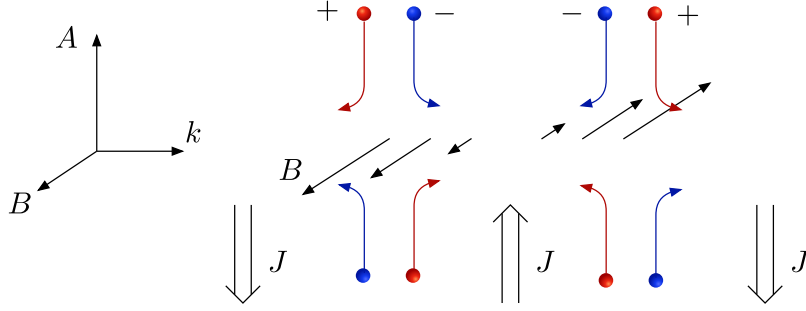


Figure 5. Illustration of a magnetic (‘Weibel’ [33]) instability for counter-propagating streams (see Section 2.3). The transverse magnetic field B bends the trajectories of charged particles in the streams (which are travelling upwards and downwards), creating current sheets (indicated by J) [34]. These currents do work on the field via the $E \cdot J$ term (since E is in the vertical direction), enhancing the field energy and leading to an instability.

so there are growing modes, with $\max \omega_i \simeq \omega_p v_0 / c$ (attained at $k \gtrsim \max(\omega_p, m)$). The physical picture behind this instability is illustrated in Figure 5. A transverse magnetic field bends the trajectories of particles in the streams, creating current sheets in the stream direction. These currents do work on the electric field, growing the instability.

More generally, if the velocity distribution is separable in the x and z directions, so

$$\int dv_y f_{\pm}(v_x, v_y, v_z) = n_{\pm} g_x(v_x) g_z(v_z) \quad (2.28)$$

(assuming symmetric positive and negative species) with $\int dv_x g_x(v_x) = \int dv_z g_z(v_z) = 1$, then

$$\Pi_{zz} = \omega_p^2 \left(1 + \sigma_z^2 \int dv_x \frac{g'_x(v_x)}{\omega/k - v_x} \right) \equiv \omega_p^2 (1 + \sigma_z^2 G(\omega/k)) \quad (2.29)$$

where $\sigma_z^2 = \int dv_z v_z^2 g_z(v_z)$ and $\omega_p^2 = 2q_{\pm}^2 n_{\pm} / m_{\pm}$, and G is defined as in appendix B. We also have $\Pi_{zx}, \Pi_{xz} \propto \int dv_z v_z g_z(v_z)$, so to simplify the analysis, we can make Π diagonal by boosting in the z direction so that $\bar{v}_z = \int dv_z v_z g_z(v_z) = 0$.

For the case of a Maxwellian velocity distribution g_x , we have (for u with positive imaginary part)

$$G(u) = - \frac{1 + \frac{u}{\sqrt{2}\sigma_x} Z\left(\frac{u}{\sqrt{2}\sigma_x}\right)}{\sigma_x^2} \quad (2.30)$$

where $Z(x) \equiv i\sqrt{\pi}e^{-x^2}\text{erfc}(-ix)$ is the plasma dispersion function [29] (inserting this into equation 2.29 reproduces the dispersion relation given in the original paper of Weibel [33]).⁵

From the dispersion relation

$$\omega^2 - k^2 - m^2 = \omega_p^2 (1 + \sigma_z^2 G(\omega/k)) \quad (2.32)$$

⁵To understand the parametric behaviour of the response function, it can also be useful to consider simpler situations, e.g. a top-hat velocity distribution, for which

$$G(u) = \frac{1}{2\sigma_x} \int_{-\sigma_x}^{\sigma_x} dv_x \frac{1}{(v_x - u)^2} = \frac{1}{u^2 - \sigma_x^2} \quad (2.31)$$

we can find that for a Maxwellian v_x distribution, an instability exists for $k \leq k_{\max}$, where

$$k_{\max}^2 = \omega_p^2 \left(\frac{\sigma_z^2}{\sigma_x^2} - 1 \right) - m^2 \quad (2.33)$$

If the RHS is negative, then there is no instability.

In many astrophysical situations, the velocity anisotropy will be small, $\sigma_z/\sigma_x \simeq 1$. In this case, we can expand the plasma dispersion function in small ω_i , and obtain (for a massless mediator)

$$\max \omega_i \simeq \sqrt{\frac{8}{27\pi}} \omega_p \sigma_z \left(\frac{\sigma_z^2}{\sigma_x^2} - 1 \right)^{3/2} \quad (2.34)$$

which is attained at $k \sim \left(\frac{\sigma_z^2}{\sigma_x^2} - 1 \right)^{1/2} \omega_p / \sqrt{3}$. This expansion is valid when $\frac{\sigma_z^2}{\sigma_x^2} - 1 \ll 1$.

For a mediator appreciably lighter than the threshold mass $\omega_p \left(\frac{\sigma_z^2}{\sigma_x^2} - 1 \right)^{1/2}$, the same ω_i expression will hold approximately.

Comparing these results to the electrostatic instabilities we discussed previously, the mass range in which instabilities existed for a two-stream velocity distribution was $m \lesssim \omega/v_{\text{th}}$. Consequently, in a scenario such as a cluster collision, the magnetic instability is present for a smaller range of mediator masses (though it can be present for other velocity distributions where electrostatic instabilities do not exist). When both instabilities are present, the parametric growth rate $\omega_i \sim \omega_p v/c$, as compared to $\omega_i \sim \omega_p$ for an electrostatic instability, means that magnetic instabilities grow slower in non-relativistic plasmas. This is illustrated in Figure 1, for which the computation includes instabilities of all types. While for some k (e.g. $k \parallel x$) the fastest-growing instability will be magnetic, the closing velocity of $\sim 10^{-3}c$ means that these growth rates are too small to be visible on the plot.

3 Astrophysical systems

As discussed in the Introduction, our goal in this paper is not to fully calculate the consequences of DM self-interactions. Instead, our aim is to identify the parameter space in which self-interactions are likely to be significant, so that future work can investigate this space more thoroughly, and in particular, identify whether there are observational consequences.

To map out this parameter space, we want to identify the astrophysical systems where, as we increase the mediator coupling from zero, the first significant effects arise. In this section, we identify different classes of candidate systems — cluster collisions, subhalos within larger halos, and halos with anisotropic velocity distributions — and discuss their properties.

Cluster collisions, as observed in systems such as the Bullet Cluster, are standard laboratories for constraining DM self-interactions [2]. The ionised gas in each cluster interacts during the collision, through SM plasma processes. In contrast, the post-collision DM distribution, as mapped out by gravitational lensing, is compatible with no non-gravitational interactions [1, 2].

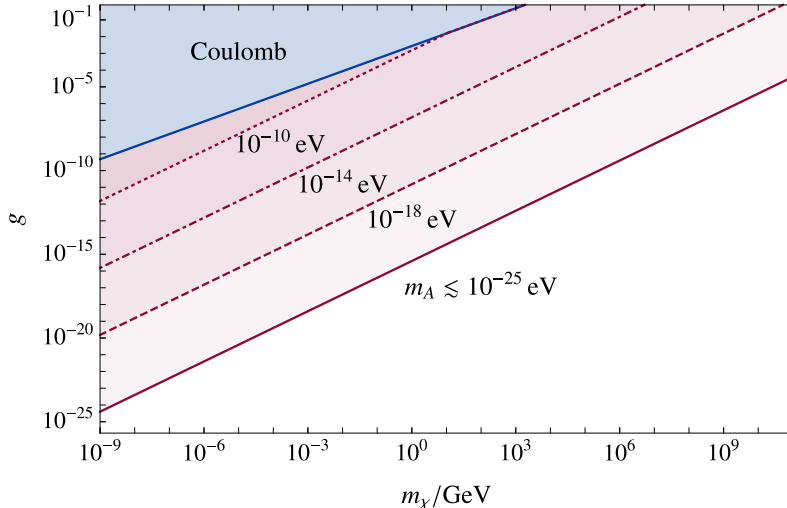


Figure 6. Estimated parameter space for which small perturbations would experience significant growth in astrophysical systems, for a vector mediator of mass m_A , coupling to DM particles of mass m_χ with coupling g . The shaded parameter space above the broken red lines, labelled with mediator mass m_A , is the space in which perturbations would grow for that mediator mass. The region above the solid red line is the region in which perturbations would grow for sufficiently light mediators. The astrophysical situations we consider are cluster collisions such as the Bullet Cluster, and dense DM subhalos (such as dwarf galaxies) moving through a larger halo (see Section 3). The ‘Coulomb’ region shows the parameter space in which $2 \rightarrow 2$ Coulomb collisions would have a significant impact in DM halos (see section 5.1). Note that, for DM masses $m_\chi \lesssim \text{eV}$, the DM occupation number in Galactic halos must be large, which may result in additional coherent scattering effects (Section 6).

To estimate when DM-DM plasma instabilities would arise during such collisions, we need some model for the DM distributions in the colliding clusters. [16] estimates these distributions, for the Bullet Cluster collision, using gravitational lensing information. Assuming cored DM density profiles⁶, their best-fit parameters have core radii $\sim 100 \text{ kpc}$, and central densities $\sim \text{few} \times 0.1 \text{ GeV cm}^{-3}$, with inferred halo velocity dispersions of $\sigma \sim 800 \text{ km s}^{-1}$. Simulations of the gas dynamics in the collision suggest that the relative velocity of the halos is $\sim 3000 \text{ km s}^{-1}$ [2]. These parameters give a central plasma frequency of

$$\omega_p = \sqrt{\frac{g^2 \rho_\chi}{m_\chi^2}} \simeq 4 \times 10^{-7} \text{ yr}^{-1} \sqrt{\frac{\rho_\chi}{0.1 \text{ GeV cm}^{-3}}} \frac{\text{GeV}}{m_\chi} \frac{g}{10^{-17}} \quad (3.1)$$

compared to a crossing time of $\sim 100 \text{ kpc}/(3000 \text{ km s}^{-1}) \sim 3 \times 10^7 \text{ yr}$. If we take a conservative threshold of $\mathcal{O}(100)$ e -folding times, we would expect plasma instabilities to grow significantly for

$$g \gtrsim 10^{-16} \frac{m_\chi}{\text{GeV}} \quad (3.2)$$

⁶profiles with central cusps, such as NFW, would lead to higher central DM densities — to be conservative, we consider cored profiles (gravitational lensing data does not have the spatial resolution to distinguish these possibilities).

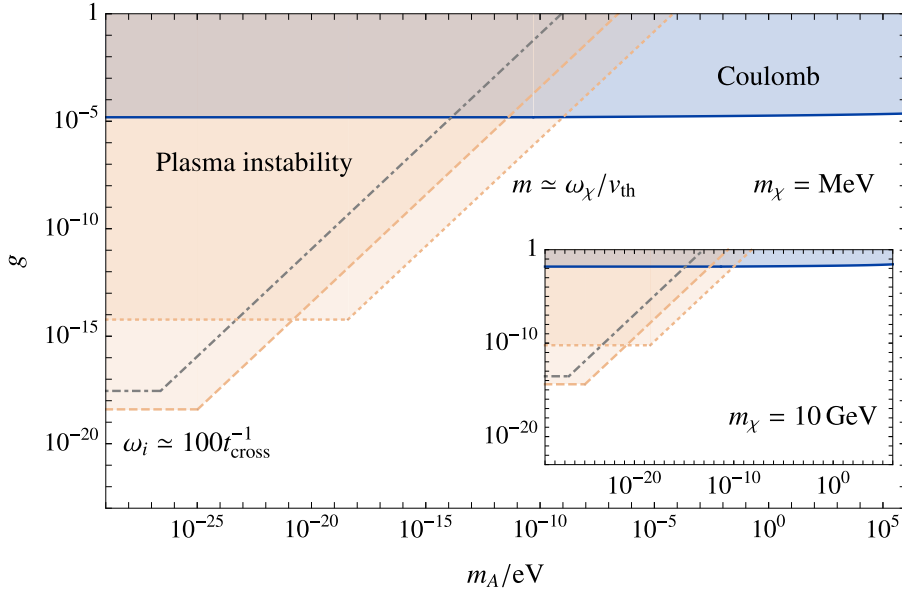


Figure 7. Estimated parameter space for which small perturbations would experience significant exponential growth in astrophysical systems, for a vector mediator of mass m_A , coupling to DM particles of mass m_χ with coupling g . In this plot, we fix $m_\chi = \text{MeV}$, and vary m_A (the inset plot shows $m_\chi = 10 \text{ GeV}$). The dashed curve corresponds to the parameter space in which instabilities would grow in a Bullet Cluster-like collision, while the dotted curve corresponds to the parameter space in which instabilities would grow for a dwarf-galaxy-like subhalo moving through a galactic halo, as discussed in Section 3. The dot-dashed grey line shows the estimated instability region for magnetic instabilities, in halos with anisotropic velocity distributions. The horizontal parts of these curves are set by the growth rate of the instability being fast compared to the crossing time in the system, while the sloping parts are set by the mediator mass being small enough for instabilities to exist. The ‘Coulomb’ region shows the parameter space in which $2 \rightarrow 2$ Coulomb collisions would have a significant impact in DM halos (see section 5.1). The inset illustrates how these regions move to higher couplings as m_χ increases; the threshold g values for the plasma instabilities increase $\propto m_\chi$, while the Coulomb threshold value increases approximately as $\propto m_\chi^{3/4}$.

if the vector mediator is sufficiently light. The latter condition should be met for

$$m \lesssim \frac{\omega_p}{\sigma} \simeq 3 \times 10^{-26} \text{ eV} \sqrt{\frac{\rho_\chi}{0.1 \text{ GeV cm}^{-3}}} \frac{800 \text{ km s}^{-1}}{\sigma} \frac{\text{GeV}}{m_\chi} \frac{g}{10^{-16}} \quad (3.3)$$

The corresponding region in m_χ, g parameter space is illustrated in Figure 6 (for various m_A), and in m_A, g parameter space (for fixed m_χ) in Figure 7. Compared to constraints from $2 \rightarrow 2$ Coulomb scatterings, discussed in Section 5.1, plasma instabilities could be important at far smaller couplings, for light enough mediators (though their observational consequences need further investigation — see Section 3.1). From equations 3.2 and 3.3, the threshold for the mediator mass to alter the parameter space in which perturbations grow is $m \gtrsim \text{few} \times 10^{-26} \text{ eV}$, basically independent of m_χ .

For a two-stream instability, the wavevector for the fastest-growing mode (with a massless mediator) has $k \sim \frac{\omega_p}{v_0} \sim \text{few} \times \frac{\omega_i}{v_0}$. For the threshold coupling we considered,

which has $\omega_i \sim \mathcal{O}(100)/t_{\text{cross}} \sim \mathcal{O}(100)v/R_{\text{cross}}$, this implies that $k \sim \mathcal{O}(100)/R_{\text{cross}}$. Consequently, the wavelength of the growing modes is small compared to the scale of the DM halo. If the DM halo is smooth, then our approximation of a spatially-uniform, freely-falling plasma should be a reasonable one (though more careful analysis, and potentially simulations, would be necessary to confirm this). For a massive mediator, the k of the fastest-growing modes is even higher. On the other hand, if the DM halo has significant substructure, e.g. a dense central spike, or a large number of ‘miniclusters’, this may have important effects.

For more massive mediators, we are limited by the $m \lesssim \omega_\chi/v_{\text{th}}$ condition on the existence of an instability. To maximise the mass range we can cover, we want DM systems with large n_χ and small v_{th} . Of the DM systems we have observational evidence for, the most extreme values of both n_χ and v_{th} are obtained in small subhalos of galactic halos, such as DM-dominated dwarf galaxies. Even assuming cored dark matter profiles, these can have central DM densities of $\gtrsim 10 \text{ GeV cm}^{-3}$ and velocity dispersion $\sim 10 \text{ km s}^{-1}$ [35–37] (though it should be mentioned that some studies claim that Milky Way dwarf galaxies may contain no dark matter at all [38, 39]). These parameters correspond to a plasma frequency of

$$\omega_p \simeq 4 \times 10^{-6} \text{ yr}^{-1} \sqrt{\frac{\rho_\chi}{10 \text{ GeV cm}^{-3}}} \frac{\text{GeV}}{m_\chi} \frac{g}{10^{-17}} \quad (3.4)$$

and a maximum mediator mass (see section 2.2.1) of roughly

$$m \lesssim \frac{\omega_p}{\text{few} \times \sigma} \sim 10^{-23} \text{ eV} \sqrt{\frac{\rho_\chi}{10 \text{ GeV cm}^{-3}}} \frac{10 \text{ km s}^{-1}}{\sigma} \frac{\text{GeV}}{m_\chi} \frac{g}{10^{-16}} \quad (3.5)$$

As illustrated in Figure 7, this means that for large enough g , instabilities persist up to larger m than in the cluster collisions case.

The low density and high velocity dispersion of the galactic halo in which the subhalo moves means that we are in the (hot) beam-plasma scenario, so the instability rate is suppressed by the density contrast between the halos. Taking a standard model for the Milky Way DM halo (e.g. [40]), the density at radii $\gg 10 \text{ kpc}$ is

$$\rho_{\text{DM}} \sim 0.1 \text{ GeV cm}^{-3} \left(\frac{20 \text{ kpc}}{r} \right)^3 \quad (3.6)$$

For typical dwarf galaxies at tens to hundreds of kpc from the galactic centre, this gives a MW halo density of $\sim 10^{-2} - 10^{-3} \text{ GeV cm}^{-3}$. Consequently, the maximum instability rate is

$$\omega_i \sim 0.5R\omega_p \sim 4 \times 10^{-6} \text{ yr}^{-1} \frac{R}{10^{-3}} \sqrt{\frac{\rho_\chi}{10 \text{ GeV cm}^{-3}}} \frac{\text{GeV}}{m_\chi} \frac{g}{10^{-14}} \quad (3.7)$$

In the case of cluster collisions, the available timescale for perturbation growth is set by the crossing time of the DM halos (as noted above, further investigation would be needed to understand the effect of spatial inhomogeneities in these halos). For the case of a subhalo moving through a larger halo, the crossing time (e.g. $\sim \text{kpc}/10^{-3} \sim 4 \times 10^6 \text{ yr}$) is significantly smaller than the timescale over which the subhalo’s surroundings will significantly change (e.g. $\sim 100 \text{ kpc}/10^{-3} \sim 4 \times 10^8 \text{ yr}$). Consequently, it is plausible

that perturbations can build up in the subhalo over timescales significantly longer than the crossing time. This is compatible with the fact that the group velocity of growing electrostatic perturbations, in the hot-beam case, is suppressed relative to the stream velocity, since the real part of the frequency is set by the dispersion relation for plasma oscillations. Here, we leave a proper analysis to future work, and conservatively restrict ourselves to perturbations that grow substantially during a single crossing time. With this assumption, equation 3.7 shows that for very light mediators, cluster collisions will be more prone to instabilities at smaller couplings.

The unstable modes in a beam-plasma setup have $k \sim \omega_p v_0$, and $\omega_i \sim R\omega_p$. At the threshold we took, $\omega_i \sim \mathcal{O}(100)v_0/R_{\text{cross}}$, so $k \sim R^{-1}\mathcal{O}(100)/R_{\text{cross}}$, and the separation between the mode's wavelength and the scale of the halo is larger than in the two-stream case. For more massive mediators, the threshold coupling is higher, and the fastest-growing modes have larger k (if a significant instability is present).

Cluster collisions and dense subhalos are the most obvious examples of bimodal DM velocity distributions, of the kind that lead to electrostatic instabilities. For standard DM halos, the (virialised) velocity distribution is expected to be roughly Maxwellian, so electrostatic instabilities should not be present. However, as we reviewed in Section 2.3, for light mediators, magnetic instabilities exist even for close-to-Maxwellian velocity distributions. In fact, numerical simulations indicate that DM halos may, outside their central regions, have quite anisotropic velocity distributions [41–46], with the radial velocity dispersion being ~ 1.5 times larger than the transverse ones. This could lead to Weibel-type instabilities.

As per Section 2.3, the growth rates of magnetic instabilities are velocity-suppressed, and the maximum mediator mass for which they exist is $\sim \omega_p$ (for $\mathcal{O}(1)$ velocity anisotropies) rather than $\sim \omega_p/v_{\text{th}}$. Consequently, a basic estimate of the parameter space in which they would arise within galactic halos gives a subset of the electrostatic estimate, as illustrated in Figure 7. In addition, the evidence for anisotropic DM distributions is somewhat indirect [47, 48], compared to the evidence for bimodal velocity distributions in subhalos and cluster collisions. Nevertheless, the coupling threshold estimates for cluster collisions and for anisotropic halos are quite close at small mediator masses, indicating that a more detailed investigation is worthwhile.

Bound structures in the universe most likely came about through a process of hierarchical structure formation, in which smaller structures formed first, and then merged to form successively larger structures [49]. During this process, the dark matter velocity distribution was often far from Maxwellian (e.g. during merger events), allowing instabilities to occur. In some sense, the cluster mergers that we observe are the late-time part of this process. Generically, we might expect these later events, which occur over longer timescales, to allow more time for instabilities to grow, and so to be the first that become important as we increase the coupling from zero. This is why we have focussed on such events (along with the fact that we have observations of them). These arguments are, of course, schematic, and would need to be checked more carefully.

Going further backwards in time, we can ask whether DM-DM instabilities could be important during the radiation era. We do not expect the DM velocity distribution then

to have been significantly bimodal, but it could have been slightly anisotropic, raising the possibility of magnetic instabilities. However, even being optimistic, it does not seem likely that these would be competitive with late-time systems, in terms of possessing instabilities at small couplings. Since $H \propto z^2$ then, while $\omega_p \propto n_{\text{DM}}^{1/2} \propto z^{3/2}$, the increased instability rate possible in denser environments is more than offset by the shorter instability time available, and the most favourable ratios occur at later times. Performing basic estimates at around the time of matter-radiation inequality, it seems likely that the late-universe systems we discussed above would allow instabilities at smaller couplings. There is, of course, a separate question of whether SM-DM couplings could lead to interesting early-universe behaviour — in particular, the pressure in the baryon-photon fluid makes it behave differently from DM, giving rise to a relative DM-baryon bulk velocity [50]. We leave such investigations to future work.

3.1 Observational consequences

As we have emphasised, the instability regions in Figure 7 do not represent observational constraints. Nevertheless, it is interesting to consider how one might be able to obtain constraints, at least in the close-to-threshold regime (that is, assuming that the relevant process is the first time in the evolution of the system that collisions become important, so that we can take the initial state to be the same as for collisionless CDM). For cluster collisions such as the Bullet Cluster, if plasma instabilities lead to significant momentum exchange, then we would expect the DM density, as reconstructed by lensing, to be more similar to the collisional SM gas, rather than the collisionless stars. Since, in reality, the latter case is observed, we could place constraints on such plasma instabilities.

A potential issue is that gravitational lensing measurements are compatible with $\mathcal{O}(1)$ effects on the DM halos, e.g. $\sim 30\%$ mass loss from the smaller halo [51]. Consequently, the effects of plasma instabilities would have to be not just $\mathcal{O}(1)$, but would have to introduce highly efficient momentum exchange, in order to be constrained. While our calculations have been purely at the level of small perturbations, which can be treated using a linear approximation, understanding the eventual consequences once perturbations become large would require a more complete analysis. It should be noted that the behaviour of SM matter in such collisions, which does undergo significant momentum exchange due to plasma effects [52], and DM simulations such as [19], suggest that the effects may be large enough to be visible. However, establishing this carefully would require significant extra work.

For the subhalo case, even if only a small fraction of the stream kinetic energy and/or momentum is transferred to the subhalo during one crossing, then the fact that the subhalo’s lifetime of billions of years is much longer than the crossing time (of only a few million years) means that there could be large cumulative effects. Momentum transfer would lead to an effective drag force on the DM; this could modify the distribution of SM matter bound to the halo [3, 53], and/or cause the subhalo’s orbit to decay. Kinetic energy transfer would heat up the subhalo, expanding or eventually evaporating it [3]. Due to these cumulative effects, it may be the case that subhalos provide more robust signals of DM plasma instabilities (though again, further work would be required to understand

these). While some of these effects have been considered in the context of $2 \rightarrow 2$ DM scattering [3, 53], the coherent nature of plasma instabilities means that, for light enough mediators, they may be important at much smaller DM-mediator couplings.

It is possible that, if structure formation does result in ‘cuspy’ DM profiles with significantly higher densities than we have considered here, then plasma instabilities could be important at even smaller couplings. Relatedly, it is possible that the first situations in which self-interactions are important could occur earlier in time than our example scenarios, and so change the initial conditions that we have been assuming (though, as per the discussion of structure formation and the early universe earlier in this section, there are reasons to believe that our our scenarios might be the first to become important as we increase the coupling from zero). If one is attempting to identify the observational signatures of a model, then such issues would need to be investigated carefully. Figure 7 represents a conservative estimate of the parameter space in which such investigations may be warranted; as discussed above, the true observationally-constrained region may reach either smaller or larger couplings.

For couplings significantly larger than the threshold value where self-interaction effects first become significant, the DM’s behaviour may be very complicated, with self-interactions at earlier times affecting the initial conditions for later processes. In more complicated hidden sectors than the simple model of symmetric DM that we have been assuming, large enough self-interactions can lead to the formation of neutral bound states. These ‘mirror atoms’, in analogy to electron-nucleon bound states in the SM, occur in a variety of models (e.g. [5, 54–57]), and if the ionised fraction is small enough, would not display the plasma behaviours we have investigated. Of course, they would also have different behaviour to our simple model in other settings, e.g. different scattering properties with the SM in direct detection experiments, so they do not represent a way to open up the same parameter space.

4 Millicharged DM

So far, we have considered entirely hidden-sector dynamics, with DM-SM interactions occurring only through gravity. However, in some models, DM interacts directly with SM states. An important example is ‘millicharged’ DM, which has a (small) charge under SM electromagnetism. In this case, the interaction dynamics are literally those of a usual EM plasma, with the addition of a different particle species. Millicharged particles can arise in a number of ways [58, 59] (it should be noted that models incorporating an extra hidden-sector photon have different behaviour, due to this extra mediator, as we discuss in Section 5).

Coherent scattering effects for millicharged DM, in the form of DM particles scattering off large-scale coherent EM fields, have been investigated extensively in the literature [20, 60–64]. These can be viewed as ‘one-many’ scatterings, with a single DM particle scattering off a field sourced by many SM particles, as opposed to the ‘many-many’ scatterings we have been considering. For example, [20] analyses scattering of millicharged DM with coherent magnetic fields in the ISM, finding that if $q_{\text{DM}}/m_{\text{DM}} \gtrsim 10^{-13} \text{ GeV}^{-1}$, the galactic disk

would have been spun down by interactions with the DM. [62] analyses the interactions of DM with magnetic fields in galaxy clusters, and finds a similar coupling limit, above which the DM profile would be strongly affected. While the plasma dynamics of these scenarios are complicated, and such limits should be viewed as plausible estimates rather than established constraints, they illustrate that, even for rather small couplings, one-many effects may be important.

An obvious question is whether, for even smaller couplings, ‘many-many’ scatterings of the kinds we have been considering could be important. For example, from Figure 7, for a massless hidden-sector mediator, and $m_\chi = \text{GeV}$, the electrostatic instability may be important in cluster collisions for $g \gtrsim \text{few} \times 10^{-16}$. In a purely-DM environment, such effects would be of interest. However, in most settings, the SM matter cannot be neglected. In particular, since the DM charge must be $\lll 1$ (for $m_\chi \ll 10^{13} \text{ GeV}$), the relatively large electron charge ($e \simeq 0.3$) means that SM matter will usually dominate the plasma dynamics, even when the DM number density is higher. As we discuss below, this can suppress plasma instabilities (or makes them dominantly SM-sector, so that DM scatters against SM-sourced fields as per the ‘one-many’ scenario considered above).

To take an example, we can consider a beam-plasma scenario in which the high-velocity ‘beam’ is DM-dominated, and the denser ‘plasma’ is SM-dominated. This might arise when e.g. a bound structure with DM and SM matter is passing through a DM halo. From section 2.2.1, the electrostatic instability rate is $\omega_i \sim R\omega_p \sim \frac{q^2 n_\chi}{m_\chi \omega_p}$, where q is the DM millicharge (the hot-beam limit is appropriate, as R is very small). Consequently, the instability rate is $\propto q^2$, rather than $\propto g$ as in the purely hidden-sector case.⁷ Physically, the SM matter makes the plasma ‘stiffer’, suppressing the instability. The instability rate being suppressed by two powers of the small DM charge means that one-many scattering probes, for which the momentum transfer rate is $\propto q$, are generally more powerful.

On the other hand, there may be other situations in which collective DM effects are important. An obvious example would be systems in which the SM density is small enough. Another possibility is that coherent SM fields provide a starting configuration for which collective instabilities involving the DM can arise. [21] investigates DM instabilities in supernova shock waves, finding that if the SM plasma is strongly magnetised, collective instabilities involving the DM can be important. In order for this to happen, the effect of the initial SM magnetic field on the DM trajectories must be significant, and further investigation would be required to understand whether such instabilities can occur in parameter space regions which are not already constrained by one-many scattering processes.

5 Kinetically mixed mediator

Another important class of models are those in which the hidden-sector mediator interacts with the SM sector. Of these, the simplest have the new vector interacting with a conserved SM current; interactions with a non-conserved current lead to (energy/vector mass)²-enhanced rates for production of the vector’s longitudinal mode [65], resulting in more

⁷For magnetic instabilities, we are effectively in the small-velocity-anisotropy regime, so the instability rate should be $\propto R^{3/2}$.

complicated behaviour, and strong constraints on light vectors [66–68]. The only conserved currents in the SM are $B - L$ (if neutrinos are Dirac) and EM. Couplings to $B - L$ result in a long-range fifth force between bulk matter, so we restrict ourselves to an EM coupling.

If χ does not couple directly to the massless SM photon (i.e. it does not have a millicharge), then the Lagrangian for a ‘dark photon’ mediator is

$$\mathcal{L} \supset -\frac{1}{4}F^2 - \frac{1}{4}F'^2 + \frac{1}{2}m^2A'^2 + gA'J_\chi + J_{\text{EM}}(A + \epsilon A') \quad (5.1)$$

This is equivalent to the standard ‘kinetic mixing’ interaction through the field redefinition $\hat{A} = A + \epsilon A'$, giving (to leading order in $\epsilon \ll 1$)

$$\mathcal{L} \supset -\frac{1}{4}\hat{F}^2 - \frac{1}{4}F'^2 - \frac{1}{2}\epsilon\hat{F}F' + \frac{1}{2}m^2A'^2 + gA'J_\chi + J_{\text{EM}}\hat{A} \quad (5.2)$$

(note the ϵ corrections simply modify the normalisations of these terms, rather than introducing new ones). Such an interaction can arise through integrating out heavier matter that couples to both A' and \hat{A} [69].

Another useful field redefinition is to define the ‘active’/‘sterile’ basis, with $\tilde{A} = A + \epsilon A'$ the ‘active’ field, and $\tilde{A}' = A' - \epsilon A$ the ‘sterile’ field (again, we assume that $\epsilon \ll 1$, and ignore normalisation changes). Then,

$$\mathcal{L} \supset -\frac{1}{4}F^2 - \frac{1}{4}F'^2 + J_{\text{EM}}\tilde{A} + gJ_\chi(\tilde{A}' + \epsilon\tilde{A}) + \frac{1}{2}m^2\tilde{A}'^2 + \epsilon m^2\tilde{A}\tilde{A}' + \frac{1}{2}\epsilon^2 m^2\tilde{A}^2 \quad (5.3)$$

If m is small compared to the appropriate scales of interest (e.g. the SM plasma mass, as we will discuss), then the m^2 mass-mixing term is small, and SM matter interacts only with \tilde{A} . This illustrates why constraints on a dark photon from SM processes decouple as $m \searrow 0$ (these constraints are shown in Figure 8).

Kinetically mixed mediators are of considerable theoretical and phenomenological interest [70]. The kinetic mixing interaction can arise from arbitrarily high scales [69], and is generically present whenever there is charged matter than interacts with the hidden sector and SM. Phenomenologically, the effectively medium-dependent coupling of the dark photon to SM matter enables models to access parameter space that would otherwise be constrained [71]. This latter point will be important for models targeted by low-threshold DM direct detection experiments, as we discuss in section 5.

5.1 Existing constraints

Some papers in the literature (e.g. [20]) claim that the ‘one-many’ bounds from DM scattering off coherent SM fields, as discussed in section 4, apply in the case of a ‘sufficiently light’ massive dark photon. However, unless the DM interacts directly with the massless SM photon, the threshold for ‘sufficiently light’ is very small. If the coupling is entirely through the kinetic mixing term, then we can see from equation 5.1 that χ interacts only with the massive A' field, which decays exponentially at distances $\gtrsim m^{-1}$ from sources. Consequently, if an SM magnetic field is sourced by currents on a scale $L \gg m^{-1}$, then the corresponding B' field is suppressed by $\sim (mL)^{-1}$ compared to B (since it is dominantly

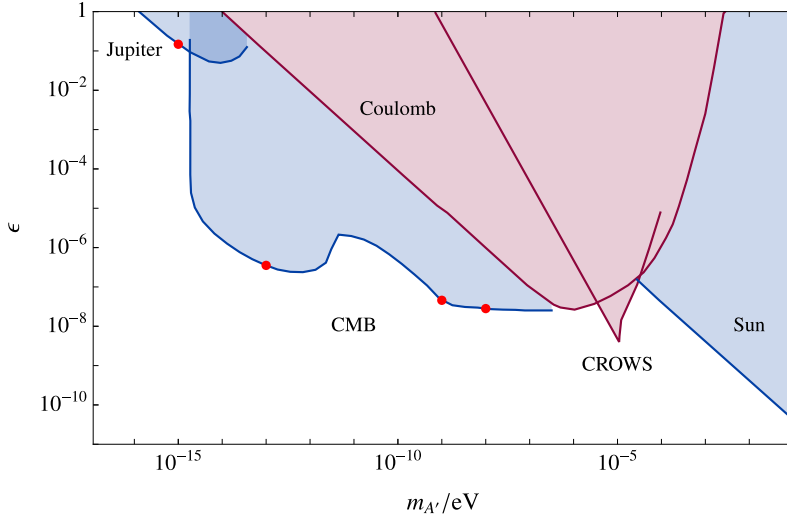


Figure 8. Constraints on a dark photon of mass $m_{A'}$, possessing a kinetic mixing ϵ with the SM photon. These constraints do not assume anything about the coupling of DM to the dark photon, relying only on SM processes (astrophysical constraints are plotted in blue, and laboratory constraints in red). The constraints come from Jupiter’s magnetic field [72], CMB observations [73], laboratory tests of Coulomb’s law [74, 75], the CROWS microwave cavity experiment [76], and stellar cooling bounds [77]. The red dots correspond to the dark photon masses illustrated in Figure 10.

sourced by currents within a range $\sim m^{-1}$). For the galactic magnetic fields considered in [20], which have coherence length $\sim \text{kpc}$, this suppression is $\sim 10^{-11}\epsilon \left(\frac{10^{-15} \text{ eV}}{m}\right)$, where the nominal $m = 10^{-15} \text{ eV}$ value is small enough to alleviate almost all constraints on ϵ from SM processes (see Figure 8). This illustrates that ‘small’ masses by particle physics standards can nevertheless be high enough to very significantly alleviate millicharge-type constraints.

The $2 \rightarrow 2$ DM-DM scattering constraints for a dark photon mediator can be estimated from modified versions of the Coulomb scattering calculations in [13, 24]. Since we are most interested in these constraints for $m \gtrsim \omega_p/v_{\text{th}}$, where plasma instabilities are suppressed, the mediator’s Compton wavelength will be smaller than the Debye length, $\lambda_D \sim v_{\text{th}}/\omega_p$. This means that the maximum impact parameter for Coulomb collisions is set by m^{-1} , rather than λ_D^{-1} , so the Coulomb logarithm is reduced compared to the massless mediator case.⁸ There are a number of disagreements between [13] and [24] regarding the details of the Coulomb scattering calculation; we will not attempt to resolve these issues, but will use the (more conservative) expressions from [24], with a modified Coulomb logarithm. This

⁸In [24], it is claimed that, for a two-species plasma with equal masses and opposite charges, the appropriate maximum impact parameter in the Coulomb logarithm is the interparticle spacing $n^{-1/3}$, rather than λ_D (in the case of a massless mediator), if $n^{-1/3} < \lambda_D$. This does not agree with the results of standard scattering integrals (e.g. [78]), or analyses of electron-positron plasmas [79]. Conversely, [13] does not take into account collective effects at all, and takes the maximum impact parameter to be set by the Galactic radius. For a massless mediator, the Coulomb logarithm will be set by λ_D , between these two results.

gives a relaxation time, through Coulomb collisions, of

$$\tau_{\text{iso}} = \frac{3}{16\sqrt{\pi}} \frac{m_\chi^3 v^3}{\alpha_\chi^2 \rho_\chi} \frac{1}{\log \Lambda_C} \quad (5.4)$$

where $\alpha_\chi \equiv g_\chi^2/(4\pi)$, and $\Lambda_C \simeq \frac{m_\chi v^2}{\alpha_\chi m_{A'}}$ (for $\omega_\chi/v \lesssim m_{A'} \lesssim m_\chi/v$). To avoid making DM too collisional, we need $\tau_{\text{iso}} \lesssim$ few Gyr in galaxies [24], which gives a bound

$$g \lesssim 2 \times 10^{-5} \left(\frac{m_\chi}{\text{MeV}} \right)^{3/4} \left(\frac{40}{\log \Lambda_C} \right)^{1/4} \quad (5.5)$$

where we have taken a typical value of the Coulomb logarithm (Λ_C will depend on g, m_χ and $m_{A'}$, but these effects will not be large). As mentioned in Section 3, it would require further analysis to determine whether all couplings above this bound are constrained, since strong enough self-interactions could lead to very complicated behaviour. However, in the absence of bound state formation (which, in the symmetric DM model we are considering, would lead to annihilation), it seems likely that frequent collisions would not be compatible with observations.

5.2 Plasma instabilities

In a situation with no charged SM matter, the growth of plasma instabilities would be exactly as in the massive-mediator case treated in Section 2. To understand how the presence of SM matter affects this, we can analyse the coupled equations of motion for Fourier modes of the vector fields,

$$\left(\begin{pmatrix} \omega^2 - k^2 & 0 \\ 0 & \omega^2 - k^2 - m^2 \end{pmatrix} - \begin{pmatrix} \Pi & \epsilon\Pi \\ \epsilon\Pi & \epsilon^2\Pi \end{pmatrix} - \begin{pmatrix} 0 & 0 \\ 0 & \Pi_\chi \end{pmatrix} \right) \begin{pmatrix} A \\ A' \end{pmatrix} = 0 \quad (5.6)$$

Here, Π is the self-energy contribution from charged SM matter, while Π_χ is from the DM (for electrostatic oscillations, we can reduce this six-dimensional system to a two-dimensional one, so that the equations below become scalar equations). For a null eigenvector (A, A') , and writing $K^2 \equiv \omega^2 - k^2$, we have $(K^2 - \Pi)A = \epsilon\Pi A'$; using this in the A' equation, we have

$$(K^2 - \Pi)(K^2 - m^2 - \epsilon^2\Pi - \Pi_\chi)A' = \epsilon^2\Pi^2 A' \quad (5.7)$$

where $K^2 \equiv \omega^2 - k^2$. In the DM-only case, we have $(K^2 - m^2 - \Pi_\chi)A' = 0$. Using the ansatz $(K^2 - m^2 - \Pi_\chi)A' = (\epsilon^2\Pi + G)A'$, equation 5.7 becomes

$$(K^2 - \Pi)GA' = \epsilon^2\Pi^2 A' \quad \Rightarrow \quad GA' = (K^2 - \Pi)^{-1} \epsilon^2\Pi^2 A' \quad (5.8)$$

If the SM charge density is appreciable, and the DM-mediator coupling is $g \ll 1$, then the SM plasma self-energy may be much larger than the DM contribution Π_χ . If our solution is a small perturbation of the DM-only case, so $K^2 A' \simeq (m^2 + \Pi_\chi)A'$, then Π being much larger than $m^2 + \Pi_\chi$ allows us to expand the $(K^2 - \Pi)^{-1}$ term in equation 5.8 by treating K^2 as small, giving

$$(K^2 - m^2 - \Pi_\chi)A' \simeq -\epsilon^2 (K^2 + K^4\Pi^{-1} + \dots) A' \quad (5.9)$$

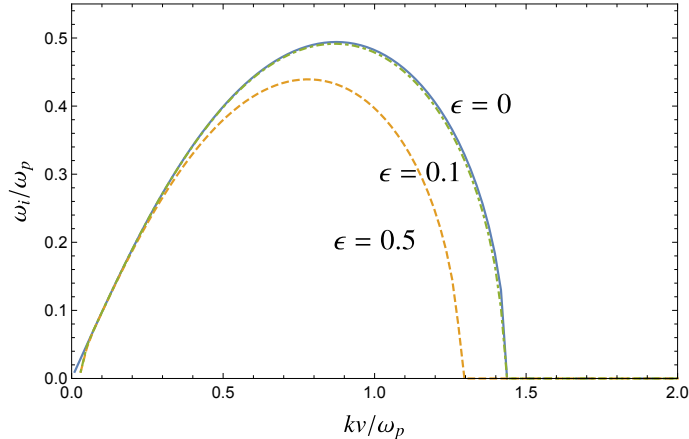


Figure 9. Longitudinal instability rate for the two-stream velocity distribution from Figure 1, for DM interacting via a light mediator that is kinetically mixed with the SM photon (Section 5). The SM plasma distribution is taken to be cold (for simplicity), with a plasma frequency 100 times that of the DM plasma, and a collision rate of $\sim 10\omega_p$ (where ω_p is the plasma frequency of the DM plasma). The different curves show the instability rate for different kinetic mixings. As these illustrate, the effect of the SM plasma is small, despite its high density and large collision rate.

The physical intuition behind this is that the SM matter is ‘stiff’, due to its strong coupling to the photon, and so decouples from the hidden sector dynamics.

In the opposite limit, where Π can be treated as small compared to K^2 in equation 5.8, we obtain

$$(K^2 - m^2 - \Pi_\chi)A' \simeq \epsilon^2 (\Pi + \Pi^2/K^2 + \dots) A' \quad (5.10)$$

Consequently, if Π is small compared to $m^2 + \Pi_\chi$, then we again obtain behaviour close to the DM-only case. Thus, in both of these scenarios, there are modes whose behaviour is close to the DM-only case. Even when the SM and DM plasma effects are comparable, we can solve for the behaviour of the combined system (equation 5.6). The upshot of this analysis is that, in most scenarios, DM-DM plasma instabilities are important in the same parts of parameter space as they would be if the mediator was not kinetically mixed. Figure 9 demonstrates this in a particular situation, by showing the instability rate for a two-stream DM velocity distribution, in the presence of a denser, collisional SM plasma. This illustrates that, even for fairly large ϵ , the main effect is to slightly rescale the single-mediator instability behaviour, as per equation 5.9.

5.3 Dark matter parameter space

For a direct detection experiment, if $m \ll \omega_p$ in the target material (or $m \ll L^{-1}$, where L is the scale of the conductive shielding around the experiment, etc), then the interactions of a DM particle with the target can be treated as occurring via the ‘active’ \tilde{A} state (equation 5.3). Consequently, the DM scatters as if it had an effective charge $q_{\text{eff}} = \epsilon g$. Processes such as the production of $\bar{\chi}\chi$ pairs in stars, and in the early universe, also

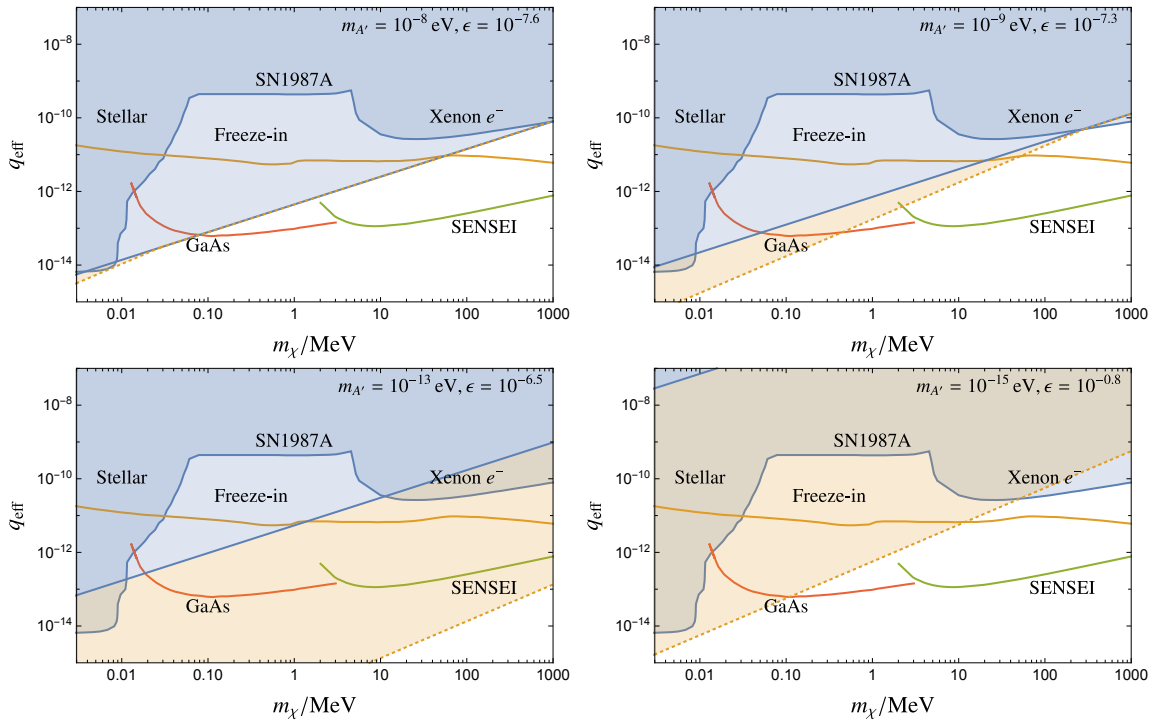


Figure 10. Constraints on the effective charge $q_{\text{eff}} \equiv \epsilon g$ of a dark matter particle χ with mass m_χ , coupling to a dark photon of mass $m_{A'}$ with coupling g , where the dark photon has a kinetic mixing ϵ with the SM photon. The dark blue shaded region corresponds to existing constraints from stellar cooling [80], from SN1987A [81], and from the Xenon10 experiment [82, 83]. The ‘freeze-in’ curve corresponds to the q_{eff} required for early-universe production from the SM radiation bath to produce the correct DM abundance [84, 85]. The SENSEI [86, 87] and GaAs [88, 89] lines correspond to projected sensitivities for future dark matter direct detection experiments. The light blue shaded regions correspond to parameter space in which $2 \rightarrow 2$ Coulomb scattering would have a significant effect in galactic halos (Section 5.1). The orange regions correspond to parameter space in which dark-sector plasma instabilities would undergo significant exponential growth in astrophysical systems, as discussed in Sections 3 and 5. The different panels correspond to different dark photon masses; for each dark photon mass, the largest kinetic mixing parameter ϵ consistent with SM constraints is assumed (illustrated in Figure 8), allowing the smallest g for a given q_{eff} . We can see that, while the smaller g permitted by smaller $m_{A'}$ relaxes the $2 \rightarrow 2$ scattering constraints, the lighter mediator mass promotes plasma instabilities.

scale with ϵg , so the effective DM parameter space, for given $m_{A'}$, is the (m_χ, q_{eff}) plane, illustrated in the plots of Figure 10.

For a given scattering cross section (set by q_{eff}), we can decrease the required g by increasing ϵ . A major difference between a kinetically mixed mediator and others (such as $B - L$ mediator, or a scalar), is that we can increase the SM coupling ϵ all the way up to $\mathcal{O}(1)$ by taking $m_{A'}$ small enough; as discussed above, the constraints on ϵ from SM processes decouple as $m \searrow 0$. These constraints are shown in Figure 8; for $m_{A'} \lesssim 10^{-16}$ eV, $\epsilon \sim \mathcal{O}(1)$ is allowed. Consequently, the $2 \rightarrow 2$ DM-DM scattering constraints discussed in Section 5.1, which are only weakly dependent on $m_{A'}$, can be significantly relaxed, to

the point where they do not constrain parameter space. This is illustrated quantitatively in Figure 10, where the different panels show the effect of decreasing $m_{A'}$ and increasing ϵ . As noted in Section 5.1, while the $m_{A'}$ required are small on particle physics scales, they are still significantly larger than the inverse length scales of astrophysical magnetic fields, so such models evade millicharge-type constraints. For other light mediators, strong constraints on the SM coupling from e.g. stellar cooling, or fifth force tests, significantly reduce the maximum allowed scattering cross-section in laboratory experiments. This generally results in near-term experiments having no realistic prospects of detecting such DM models, at least for DM masses $\lesssim 10$ MeV [71].

However, since we must go to rather small $m_{A'}$ to open up this parameter space, this raises the possibility that coherent DM-DM scattering processes become important. Figure 10 also shows the parameter space regions in which plasma instabilities will start growing in astrophysical systems. Unlike the $2 \rightarrow 2$ scattering bounds, the enhancement of instabilities due to decreased $m_{A'}$ compensates for the increased ϵ that is possible, and much of the low-mass target range is within the plasma instability region, even for $\epsilon \sim \mathcal{O}(1)$. In particular, the ‘freeze-in’ cross section [84, 85], for which thermal production of χ from the SM radiation bath is sufficient to produce the whole DM abundance, is within this regime up to $\mathcal{O}(10)$ MeV. Conversely, when $m_{A'}$ is large enough that plasma instabilities would be unimportant, then ϵ is constrained to be small, and the Coulomb scattering bounds constrain much of the target parameter space for proposed light DM detection experiments.

As we discussed in section 3, these plasma instability regions should not be viewed as observationally constrained, since it is logically possible that the growth of perturbations does not lead to observable effects. However, our calculations do motivate more careful investigations into whether these regions of parameter space are astrophysically viable. Of course, even if it turns out that such particles cannot be all of the dark matter, it is possible that $\mathcal{O}(10\%)$ of the DM mass density is strongly collisional [71]. To predict the signals of such subcomponent models at DM detection experiments, the effects of this collisionality on the DM distribution at Earth would need to be taken into account.

6 Light bosonic DM

In our discussions so far, we have assumed that dark matter can be treated as point particles, with some interparticle separation $\sim n^{-1/3}$. However, when the de Broglie wavelength of the DM becomes comparable to $n^{-1/3}$, i.e. the occupation number becomes $\gtrsim 1$, this picture breaks down. For DM in the vicinity of the Earth, this occurs at $m_{\text{DM}} \lesssim \text{eV}$. While most experiments searching for DM scattering do not cover such small masses, some types of experiments [90] and astrophysical observations [91] may have sensitivity there, and in any case, understanding the behaviour is of theoretical interest.

In the $m_{\text{DM}} \ll \text{eV}$ regime, we can treat the (necessarily bosonic) DM as a large occupation number classical field. If, before structure formation, the particle and antiparticle fields have some independent perturbations⁹, then (ignoring non-gravitational interactions) the

⁹for example, as would arise from inflationary isocurvature fluctuations, or from small-scale fluctuations

virialization process will result in them becoming effectively independent Gaussian random fields in halos, with characteristic wavelength $\lambda_B \sim 1/(m_{\text{DM}}v)$. If we consider a particular spatial point, then the amplitude of the particle field will generically be $\mathcal{O}(1)$ different from that of the antiparticle field. Supposing that the amplitude of the particle field is larger, then there is a net positive charge density over a spatial scale $\sim \lambda_B$. In charge density terms, the particle and antiparticle fields result in an array of charged ‘blobs’, each of typical size $\sim \lambda_B$, and typical charge $\sim \pm n_{\text{DM}}\lambda_B^3$.

If λ_B is significantly smaller than the wavelength of perturbations that would grow in a uniform plasma, then the smooth approximations that we used above will be valid (c.f. the discussion around equation 2.13). If not, then a modified treatment would be required. For a two-stream velocity distribution, and a light mediator, the wavenumber of the most unstable perturbations is $k \sim \omega_p/v$, so at the threshold coupling from equation 3.2, and taking the nominal cluster collision parameters from Section 3,

$$\lambda_B \ll k^{-1} \quad \Leftrightarrow \quad (6.1)$$

$$m_{\text{DM}} \gg \frac{(g/m_{\text{DM}})\rho^{1/2}}{v^2} \sim 10^{-24} \text{ eV} \left(\frac{\rho}{0.1 \text{ GeV cm}^{-3}} \right)^{1/2} \left(\frac{g/m_{\text{DM}}}{10^{-16} \text{ GeV}^{-1}} \right) \left(\frac{3000 \text{ km s}^{-1}}{v} \right)^2$$

Bearing in mind that the DM mass must be $\gtrsim 10^{-21}$ eV to be compatible with small scale structure observations [92], we see that for a light enough mediator, significantly above-threshold couplings would be required to affect the plasma instability behaviour. For a heavier mediator, the perturbation wavenumber near the coupling threshold is $k \sim m_{A'}$, so we need $m_{\text{DM}} \gg m_{A'}/v$ there for the smooth plasma description to be accurate.

For a heavy enough mediator and small enough coupling, plasma instabilities will be suppressed. However, ‘collisional’ effects on the plasma evolution will still exist, and will no longer be well modelled as $2 \rightarrow 2$ Coulomb collisions. Instead, ‘blob-blob’ collisions will occur coherently (this is in direct analogy to the picture of gravitational relaxation for light bosonic DM [92–94]). Treating scattering off a blob via standard scattering theory [95], the scattering rate (for a single DM particle) will be parametrically set by

$$\Gamma \sim \sigma v n_B \sim \frac{g^4 N_B^2}{16\pi m_{\text{DM}}^2 v^4} v n_B \log \Lambda_C \sim \frac{\log \Lambda_C}{16\pi} \frac{g^4 \rho^2}{m_{\text{DM}}^7 v^6} \quad (6.2)$$

where $N_B \sim n_{\text{DM}}\lambda_B^3$ is the number of particles in a blob, $n_B \sim \lambda_B^{-3}$ is the number density of blobs, and $\log \Lambda_C$ indicates the appropriate Coulomb logarithm. This form will be valid if $m_{A'} \lesssim m_{\text{DM}}v$, so that the mediator is long-range compared to the blob size.¹⁰ Equation 6.2 has the same density and velocity dependence as for gravitational relaxation of light bosonic DM, but differs from the $2 \rightarrow 2$ Coulomb collisions rate (equation 5.4), which may result in stronger constraints than the latter at small m_{DM} .

arising from a phase transition production mechanism. We leave the question of how large such fluctuations need to be for future work.

¹⁰If the mediator is short-range compared to the de Broglie wavelength, then the behaviour will be as per a contact interaction, giving

$$\Gamma \sim \frac{1}{16\pi} \frac{g^4 \rho^2}{m_{A'}^4 m^3 v^2} \quad (6.3)$$

(the constant factor here should be not taken seriously). Similar parametric behaviour would occur for e.g.

As an example, we can consider parameters motivated by the experiment proposed in [90]. If we take $m_{\text{DM}} = 10^{-4}$ eV, so that the de Broglie wavelength is not larger than the detector, and $m_{A'} = 10^{-7}$ eV, giving a mediator range on the same scale, then for $g \lesssim 5 \times 10^{-14}$, astrophysical plasma instabilities are suppressed (according to our estimates in Section 3). If we naively applied the $2 \rightarrow 2$ Coulomb constraints from Section 5.1, these would give $g \lesssim 6 \times 10^{-13}$. However, if we take the estimate of the coherent scattering rate from equation 6.2, and set $\Gamma \sim 1/\text{Gyr}$ as a rough constraint, this would give

$$g \lesssim 4 \times 10^{-17} \left(\frac{\text{GeV cm}^{-3}}{\rho} \right)^{1/2} \left(\frac{v}{10^{-3}} \right)^{3/2} \quad (6.5)$$

Consequently, the coherence-enhanced scattering rate is more significant than plasma instabilities in this regime, and potentially more constraining than a naive application of the $2 \rightarrow 2$ Coulomb scattering bounds.

Despite these rates, it is unclear whether coherent scattering processes of these kinds will provide observational constraints. One issue is that, if the scatterings drive the particle and antiparticle fields towards identical spatial profiles, then we will no longer have charged blobs. Consequently, it is not obvious whether the scattering process will saturate before it has observable effects on halo shapes.

For light enough mediators ($m_{A'} \lesssim m_{\text{DM}}v^2$), it would also be necessary to check whether coherent emission of the mediator is ever important. While particle-antiparticle annihilation to the mediator is possible when $2m_{\text{DM}} \geq m_{A'}$, the rate of this process is $\propto g^4$, so would likely be unimportant (there will be a rate $\propto g^2$ from ‘off-shell’ parts of the DM field’s wavefunction, due to it being bound in a gravitational potential, but these will be extremely small in a typical halo).

These caveats illustrate that more investigation would be needed to understand the observational consequences of light bosonic DM interacting via a light vector mediator. However, our estimates in this section do suggest that coherent effects may be important in new regions of parameter space.

7 Conclusions

As we have emphasised throughout, the goal of our paper has not been to constrain models of self-interacting DM, but to map out parameter space regions in which long-range coherent self-interactions may be important. The obvious follow-on would be to more carefully investigate the physics of these models, and to determine whether they are observationally constrained. One of the most important models is the kinetically mixed mediator scenario,

a scalar of mass m interacting via a quartic interaction $\lambda\phi^4$, which would give

$$\Gamma \sim \frac{1}{16\pi} \frac{\lambda^2 \rho^2}{m^7 v^2} \sim \frac{1}{16\pi} \frac{\rho^2}{f^4 m^3 v^2} \quad (6.4)$$

where we have used the usual scaling of the quartic coupling $\lambda \sim m^2/f^2$ in terms of the symmetry breaking scale f , for a potential arising from high-scale breaking of a shift symmetry. This matches the parametric relaxation timescale from [96, 97].

for which it would be very interesting to determine whether the models being targeted by proposed DM direct detection experiments [86, 88, 90, 98–100] are astrophysically viable.

Even for purely hidden-sector interactions, such investigations may be quite complicated. In principle, one would like to start from the very early universe (e.g. from when the DM was produced) and track the DM’s evolution until today. Without this, one would not know the initial DM distribution in scenarios such as cluster mergers, so unless one could demonstrate that all observationally-acceptable initial conditions behave in a certain way, relating the model to observations would be difficult. Of course, in practice, it would hopefully be possible to make significant approximations, e.g. that self-interactions have negligible effects before a certain point, or conversely, that they effectively thermalise the distribution. SM plasma behaviour may provide some guide, at least in the regime of a light mediator and strong coupling.

As well as understanding the constraints that could be obtained from plasma instabilities, it would be useful to understand the observational signatures that could arise, in models with a coupling that is just large enough. The discussion in Section 3.1 represents a first attempt in this direction. In particular, understanding the relationships between observational signatures in different astrophysical systems would be important. For DM that is not super-heavy, such threshold-level couplings would need to be extremely small — however, there are potential theoretical reasons why such couplings might arise [101].

There are many dark matter models which feature long-range vector mediators, beyond the simple examples we have considered. The most obvious examples are models with additional species, having different charges and/or masses [5, 23] (such as the proton and electron in the SM). If most of the present-day dark matter is ionized (i.e. consists of isolated charged particles), then analogues of the plasma calculations we have carried out here will apply, though the presence of different-mass species will change the behaviour in potentially-interesting ways (c.f. ion effects in SM plasmas). On the other hand, if dark matter is dominantly in the form of overall-neutral bound states (‘dark atoms’), then the interactions between these will be effectively short-ranged, and will not give rise to plasma instabilities.

As mentioned in Section 3, it may be observationally viable for a $\sim \mathcal{O}(10\%)$ subcomponent of DM to be strongly self-interacting [71]. At the threshold of viability, there may be interesting observational effects of long-range interactions in such a subcomponent. In section 1.2, we briefly reviewed [18, 19, 102], which simulated the dynamics of a DM subcomponent interacting via a massless hidden-sector mediator. Other questions, including the DM distribution at Earth of a subcomponent [26], would also be interesting to consider, and relevant to the direct detection phenomenology of such a subcomponent.

Acknowledgments

We acknowledge helpful conversations with Prateek Agrawal, Asimina Arvanitaki, Daniel Egana-Ugrinovic, Peter Graham, Tongyan Lin, and Julian Munoz, and thank Jung-Tsung Li and Tongyan Lin for comments on a draft of this paper. RL’s research is supported in

part by the National Science Foundation under Grant No. PHYS-1720397, and the Gordon and Betty Moore Foundation Grant GBMF7946.

A Maxwellian velocity distribution

Virialised DM halos are expected to have approximately Maxwellian velocity dispersions, and the dispersion relations for these can be treated analytically. For a Maxwellian velocity distribution

$$f(v) = \frac{1}{(2\pi\sigma^2)^{3/2}} e^{-v^2/(2\sigma^2)} \quad (\text{A.1})$$

we have

$$\Pi A = \begin{pmatrix} -\omega_p^2 \frac{\omega}{\sqrt{2}k\sigma} Z\left(\frac{\omega}{\sqrt{2}k\sigma}\right) & 0 \\ 0 & -(\omega^2 - k^2) \frac{\omega_p^2}{k^2\sigma^2} \frac{\omega}{\sqrt{2}\sigma k} \left(Z\left(\frac{\omega}{\sqrt{2}k\sigma}\right) + \sqrt{2} \frac{k\sigma}{\omega} \right) \end{pmatrix} \begin{pmatrix} A_\perp \\ A_\parallel \end{pmatrix} \quad (\text{A.2})$$

where Z is the plasma dispersion function [29]. This gives the usual small- k expansion of the non-relativistic dispersion relations [31]. To find the response function for a velocity distribution with non-zero mean velocity, we can we perform the appropriate Lorentz boost.

Another relevant limit of the Maxwellian self-energy is the $\omega \rightarrow 0$ limit, for which we have

$$\Pi A \rightarrow \begin{pmatrix} 0 & 0 \\ 0 & \omega_p^2/\sigma^2 \end{pmatrix} \begin{pmatrix} A_\perp \\ A_\parallel \end{pmatrix} \quad (\text{A.3})$$

This shows that static magnetic fields are not screened, while electric fields are screened over the Debye length scale $\lambda_D \sim (\omega_p/\sigma)^{-1}$.

B Penrose stability criteria

In this appendix, we review the Penrose stability criteria [32] for electrostatic plasma oscillations, and extend them to the case of a massive vector mediator.

From section 2.2, the dispersion relation for an electrostatic perturbation is

$$(c^2 k^2 + c^4 m^2) \simeq c^2 \sum_s \frac{q_s^2}{m_s} \int d^3 v \frac{k \cdot \partial_v f_s}{k \cdot v - \omega} \quad (\text{B.1})$$

Considering a single species for simplicity (or equivalently, symmetric positive and negative charges), we can define $v_k = \hat{k} \cdot v$, and $g(v_k) = \int d^2 v_\perp f(v)/n$, where v_\perp is the velocity component perpendicular to k (so $\int dv_k g(v_k) = 1$). Then, we have

$$(k^2 + m^2 c^2) \simeq \omega_p^2 \int dv_k \frac{g'(v_k)}{v_k - \omega/k} \quad (\text{B.2})$$

where $\omega_p^2 = \sum_s q_s^2 n_s / m_s$. If we define $G(u) \equiv \int dv_k \frac{g'(v_k)}{v_k - u}$, then the dispersion relation is $G(\omega/k) = (k^2 + m^2 c^2) / \omega_p^2$. If there is a solution where ω has positive imaginary part, then that mode will be unstable to growth. For a massless mediator, it can be shown that the existence of such a growing mode is equivalent to there existing some real u for which $G(u)$

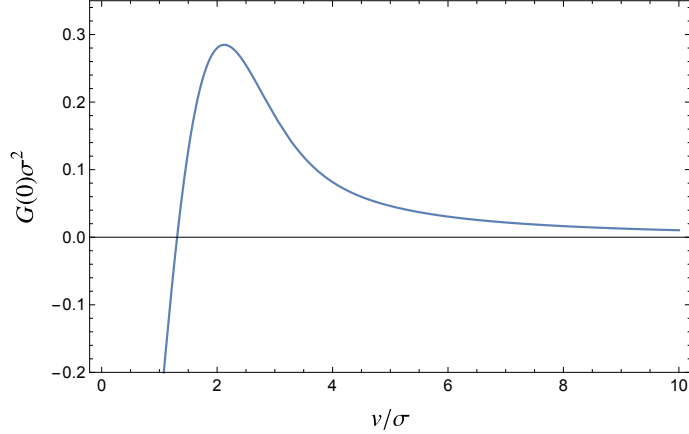


Figure 11. Normalised longitudinal self-energy for a two-Gaussian-stream velocity distribution, evaluated at zero phase velocity (see equation B.4). As discussed in appendix B, this function is related to the existence of unstable longitudinal modes.

is real and ≥ 0 (effectively, if there are growing modes, then there must be a marginally stable mode).

Since

$$G(u + i0_+) = P \int dv_k \frac{g'(v_k)}{v_k - u} + i\pi g'(u) \quad (\text{B.3})$$

to have $G(u) \geq 0$, we need $g'(u) = 0$. For the example of a symmetric ‘two-stream’ velocity distribution, where each stream is Maxwellian with velocity distribution σ , and the closing velocity is $2v$, we have

$$G(0 + i0_+) = \frac{-1 + 2 \frac{v}{\sqrt{2}\sigma} D\left(\frac{v}{\sqrt{2}\sigma}\right)}{\sigma^2} \quad (\text{B.4})$$

where D is the Dawson integral [103]. This function is plotted in Figure 11. For a massless mediator, an unstable mode exists if $G(0 + i0_+) \geq 0$, which is true for $v \gtrsim 1.3\sigma$.

For a massive mediator, the dispersion relation is

$$\frac{k^2 + c^2 m^2}{\omega_p^2} = G(\omega/k) \quad (\text{B.5})$$

By the same logic as in the massless case, an instability exists if there is some real u for which $G(u) - c^2 m^2 / \omega_p^2$ is real and non-negative. From Figure 11, we can see that this will be true only for some bounded range of v/σ , if at all. If $m^2 c^2 / \omega_p^2 \geq \max G(0 + i0_+) \simeq 0.3/\sigma^2$, then there are no solutions, and consequently no instability. In terms of the notation in Section 2.2, where ω_p labelled the plasma frequency for each stream, rather than for both streams, we need $m^2 c^2 / (2\omega_p^2) \geq G(0 + i0_+)$.

Less symmetric velocity distributions are also of interest. An example is the case of a dense, low-velocity-dispersion stream passing through a lower-density, higher-velocity-dispersion stream — the ‘beam-plasma’ scenario discussed in Section 2.2.1. This kind of

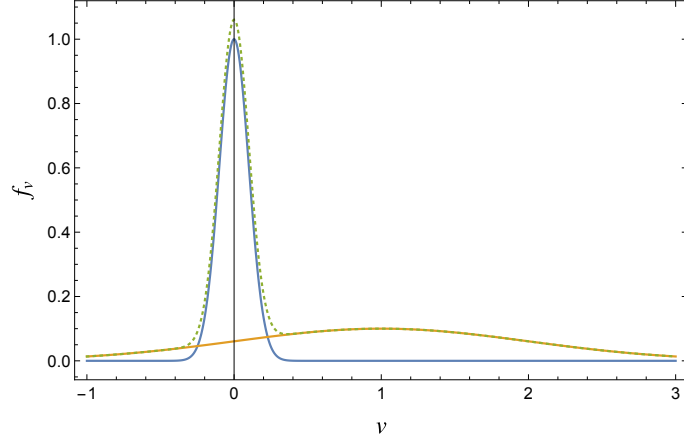


Figure 12. Velocity distribution for a ‘beam-plasma’ scenario, in which the beam velocity dispersion is $\sigma_s = 1$, the beam velocity is $v_s = 1$, the plasma velocity dispersion is $\sigma_p = 0.1$, and the density ratio is $R = 0.1$. The blue curve shows the velocity distribution of the ‘plasma’ stream, the orange curve that of the ‘beam’, and the dotted curve the combined velocity distribution.

velocity distribution is illustrated in Figure 12. If both of the streams have Maxwellian velocity distributions, and we take the denser stream to be at rest, so

$$g(v_k) \simeq \frac{1}{\sqrt{2\pi\sigma_p^2}} e^{-v_k^2/(2\sigma_p^2)} + \frac{R}{\sqrt{2\pi\sigma_s^2}} e^{-(v_k-v_s)^2/(2\sigma_s^2)} \quad (\text{B.6})$$

with $R \ll 1$, then the u for which $g'(u) = 0$ satisfies

$$u^2 \simeq 2\sigma_p^2 \log \frac{u\sigma_s^3}{v_s\sigma_p^3 R} + v_s^2 \frac{\sigma_p^2}{\sigma_s^2} \quad (\text{B.7})$$

(where we have assumed that $v_s \gg v$, which is true if $\sigma_s \gg \sigma_p$). If the beam velocity distribution is broad, so $v_s \sim \sigma_s$, then we have $u \sim C\sigma_p$, where C is at most logarithmically large. The integral for $G(u + i0_+)$ is then dominated by the ‘plasma’ peak near the origin, which (via integration by parts) is

$$G(u + i0_+) = P \int dv_k \frac{g'(v_k)}{v_k - u} = \int dv_k \frac{g(v_k) - g(u)}{(v_k - u)^2} \simeq \frac{1}{u^2} \sim \frac{1}{C^2\sigma_p^2} \quad (\text{B.8})$$

Consequently, for a massive mediator, an instability exists if

$$G(u + i0_+) \geq \frac{m^2 c^2}{\omega_p^2} \quad \Leftrightarrow \quad m^2 \lesssim \frac{\omega_p^2}{C^2\sigma_p^2} \quad (\text{B.9})$$

for some $C \sim \mathcal{O}(10)$.

References

- [1] D. Clowe, M. Bradač, A. H. Gonzalez, M. Markevitch, S. W. Randall, C. Jones et al., *A direct empirical proof of the existence of dark matter*, *The Astrophysical Journal* **648** (Aug, 2006) L109–L113.

- [2] A. Robertson, R. Massey and V. Eke, *What does the bullet cluster tell us about self-interacting dark matter?*, *Monthly Notices of the Royal Astronomical Society* **465** (Oct, 2016) 569–587.
- [3] F. Kahlhoefer, K. Schmidt-Hoberg, M. T. Frandsen and S. Sarkar, *Colliding clusters and dark matter self-interactions*, *Monthly Notices of the Royal Astronomical Society* **437** (Nov, 2013) 2865–2881.
- [4] Z. Chacko, H.-S. Goh and R. Harnik, *Natural electroweak breaking from a mirror symmetry*, *Physical Review Letters* **96** (Jun, 2006) .
- [5] I. G. García, R. Lasenby and J. March-Russell, *Twin higgs asymmetric dark matter*, *Physical Review Letters* **115** (Sep, 2015) .
- [6] T. Damour, G. W. Gibbons and C. Gundlach, *Dark matter, time-varying G , and a dilaton field*, *Physical Review Letters* **64** (jan, 1990) 123–126.
- [7] B.-A. Gradwohl and J. A. Frieman, *Dark matter, long-range forces, and large-scale structure*, *The Astrophysical Journal* **398** (Oct, 1992) 407.
- [8] A. Nusser, S. S. Gubser and P. J. E. Peebles, *Structure formation with a long-range scalar dark matter interaction*, *Physical Review D* **71** (Apr, 2005) .
- [9] M. Kesden and M. Kamionkowski, *Tidal tails test the equivalence principle in the dark-matter sector*, *Physical Review D* **74** (Oct, 2006) .
- [10] W. A. Hellwing and R. Juszkiewicz, *Dark matter gravitational clustering with a long-range scalar interaction*, *Physical Review D* **80** (Oct, 2009) .
- [11] D. Comelli, M. Crisostomi and L. Pilo, *Perturbations in massive gravity cosmology*, *Journal of High Energy Physics* **2012** (jun, 2012) .
- [12] C. Chiuderi and M. Velli, *Basics of Plasma Astrophysics*. Springer Milan, 2015, [10.1007/978-88-470-5280-2](https://doi.org/10.1007/978-88-470-5280-2).
- [13] L. Ackerman, M. R. Buckley, S. M. Carroll and M. Kamionkowski, *Dark Matter and Dark Radiation*, *Phys. Rev.* **D79** (2009) 023519, [[0810.5126](https://arxiv.org/abs/0810.5126)].
- [14] F. Chen, *Introduction to Plasma Physics and Controlled Fusion*. Springer International Publishing, 2015.
- [15] R. J. Briggs, *Two-Stream Instabilities*, *Advances in Plasma Physics* **4** (Jan., 1971) 43.
- [16] D. Paraficz, J.-P. Kneib, J. Richard, A. Morandi, M. Limousin, E. Jullo et al., *The bullet cluster at its best: weighing stars, gas, and dark matter*, *Astronomy & Astrophysics* **594** (Oct, 2016) A121.
- [17] B. Feldstein, J. Mardon and L. O’Silva, “A (nearly) weaker-than-gravity bound on dark matter electromagnetism.”
- [18] M. Heikinheimo, M. Raidal, C. Spethmann and H. Veermäe, *Dark matter self-interactions via collisionless shocks in cluster mergers*, *Phys. Lett.* **B749** (2015) 236–241, [[1504.04371](https://arxiv.org/abs/1504.04371)].
- [19] C. Spethmann, H. Veermäe, T. Sepp, M. Heikinheimo, B. Deshev, A. Hektor et al., *Simulations of Galaxy Cluster Collisions with a Dark Plasma Component*, *Astron. Astrophys.* **608** (2017) A125, [[1603.07324](https://arxiv.org/abs/1603.07324)].
- [20] A. Stebbins and G. Krnjaic, *New Limits on Charged Dark Matter from Large-Scale Coherent Magnetic Fields*, *JCAP* **1912** (2019) 003, [[1908.05275](https://arxiv.org/abs/1908.05275)].

- [21] J.-T. Li and T. Lin, *Dynamics of millicharged dark matter in supernova remnants*, *Physical Review D* **101** (May, 2020) .
- [22] D.-C. Dai, K. Freese and D. Stojkovic, *Constraints on dark matter particles charged under a hidden gauge group from primordial black holes*, *Journal of Cosmology and Astroparticle Physics* **2009** (Jun, 2009) 023–023.
- [23] J. L. Feng, M. Kaplinghat, H. Tu and H.-B. Yu, *Hidden charged dark matter*, *Journal of Cosmology and Astroparticle Physics* **2009** (Jul, 2009) 004–004.
- [24] P. Agrawal, F.-Y. Cyr-Racine, L. Randall and J. Scholtz, *Make dark matter charged again*, *Journal of Cosmology and Astroparticle Physics* **2017** (May, 2017) 022–022.
- [25] M. Garny, A. Palessandro, M. Sandora and M. S. Sloth, *Charged planckian interacting dark matter*, *Journal of Cosmology and Astroparticle Physics* **2019** (Jan, 2019) 021–021.
- [26] J. Clarke and R. Foot, *Plasma dark matter direct detection*, *Journal of Cosmology and Astroparticle Physics* **2016** (Jan, 2016) 029–029.
- [27] J. Binney and S. Tremaine, *Galactic Dynamics: (Second Edition)*. Princeton Series in Astrophysics. Princeton University Press, 2008.
- [28] D. Lynden-Bell, R. Wood and A. Royal, *The gravo-thermal catastrophe in isothermal spheres and the onset of red-giant structure for stellar systems*, *Monthly Notices of the Royal Astronomical Society* **138** (feb, 1968) 495–525.
- [29] R. Fitzpatrick, *Plasma physics : an introduction*. CRC Press, Taylor & Francis Group, 2015.
- [30] M. L. Bellac, *Thermal Field Theory*. Cambridge University Press, Aug, 1996, [10.1017/cbo9780511721700](https://doi.org/10.1017/cbo9780511721700).
- [31] G. Raffelt, *Stars as laboratories for fundamental physics: The astrophysics of neutrinos, axions, and other weakly interacting particles*. 5, 1996.
- [32] O. Penrose, *Electrostatic instabilities of a uniform non-maxwellian plasma*, *Physics of Fluids* **3** (1960) 258.
- [33] E. S. Weibel, *Spontaneously growing transverse waves in a plasma due to an anisotropic velocity distribution*, *Physical Review Letters* **2** (Feb, 1959) 83–84.
- [34] B. D. Fried, *Mechanism for instability of transverse plasma waves*, *Physics of Fluids* **2** (1959) 337.
- [35] M. G. Walker, M. Mateo, E. W. Olszewski, J. Peñarrubia, N. W. Evans and G. Gilmore, *A UNIVERSAL MASS PROFILE FOR DWARF SPHEROIDAL GALAXIES?*, *The Astrophysical Journal* **704** (Oct, 2009) 1274–1287.
- [36] J. Wolf, G. D. Martinez, J. S. Bullock, M. Kaplinghat, M. Geha, R. R. Muñoz et al., *Accurate masses for dispersion-supported galaxies*, *Monthly Notices of the Royal Astronomical Society* (May, 2010) no–no.
- [37] J. J. Adams, J. D. Simon, M. H. Fabricius, R. C. E. van den Bosch, J. C. Barentine, R. Bender et al., *DWARF GALAXY DARK MATTER DENSITY PROFILES INFERRED FROM STELLAR AND GAS KINEMATICS*, *The Astrophysical Journal* **789** (Jun, 2014) 63.
- [38] F. Hammer, Y. Yang, J. Wang, F. Arenou, M. Puech, H. Flores et al., *On the absence of*

- dark matter in dwarf galaxies surrounding the milky way, *The Astrophysical Journal* **883** (Oct, 2019) 171.
- [39] F. Hammer, Y. Yang, F. Arenou, J. Wang, H. Li, P. Bonifacio et al., *Orbital evidences for dark-matter-free milky way dwarf spheroidal galaxies*, *The Astrophysical Journal* **892** (Mar, 2020) 3.
- [40] F. Nesti and P. Salucci, *The dark matter halo of the milky way, AD 2013*, *Journal of Cosmology and Astroparticle Physics* **2013** (Jul, 2013) 016–016.
- [41] N. W. Evans and J. H. An, *Distribution function of dark matter*, *Physical Review D* **73** (Jan, 2006) .
- [42] R. Wojtak, E. L. Lokas, G. A. Mamon, S. Gottlöber, A. Klypin and Y. Hoffman, *The distribution function of dark matter in massive haloes*, *Monthly Notices of the Royal Astronomical Society* **388** (Aug, 2008) 815–828.
- [43] A. D. Ludlow, J. F. Navarro, S. D. M. White, M. Boylan-Kolchin, V. Springel, A. Jenkins et al., *The density and pseudo-phase-space density profiles of cold dark matter haloes*, *Monthly Notices of the Royal Astronomical Society* **415** (Jun, 2011) 3895–3902.
- [44] D. Lemze, R. Wagner, Y. Rephaeli, S. Sadeh, M. L. Norman, R. Barkana et al., *PROFILES OF DARK MATTER VELOCITY ANISOTROPY IN SIMULATED CLUSTERS*, *The Astrophysical Journal* **752** (Jun, 2012) 141.
- [45] M. Sparre and S. H. Hansen, *The behaviour of shape and velocity anisotropy in dark matter haloes*, *Journal of Cosmology and Astroparticle Physics* **2012** (Oct, 2012) 049–049.
- [46] R. Wojtak, S. Gottlöber and A. Klypin, *Orbital anisotropy in cosmological haloes revisited*, *Monthly Notices of the Royal Astronomical Society* **434** (Jul, 2013) 1576–1585.
- [47] O. Host, S. H. Hansen, R. Piffaretti, A. Morandi, S. Ettori, S. T. Kay et al., *MEASUREMENT OF THE DARK MATTER VELOCITY ANISOTROPY IN GALAXY CLUSTERS*, *The Astrophysical Journal* **690** (Dec, 2008) 358–366.
- [48] D. Lemze, Y. Rephaeli, R. Barkana, T. Broadhurst, R. Wagner and M. L. Norman, *QUANTIFYING THE COLLISIONLESS NATURE OF DARK MATTER AND GALAXIES IN a1689*, *The Astrophysical Journal* **728** (Jan, 2011) 40.
- [49] S. Dodelson, *Modern Cosmology*. Academic Press, Elsevier Science, 2003.
- [50] C. Dvorkin, K. Blum and M. Kamionkowski, *Constraining dark matter-baryon scattering with linear cosmology*, *Physical Review D* **89** (jan, 2014) .
- [51] M. Markevitch, A. H. Gonzalez, D. Clowe, A. Vikhlinin, W. Forman, C. Jones et al., *Direct constraints on the dark matter self-interaction cross section from the merging galaxy cluster 1e 0657-56*, *The Astrophysical Journal* **606** (May, 2004) 819–824.
- [52] M. Markevitch, *Intergalactic shock fronts*, *arxiv:1010.3660* (2010) .
- [53] F. Kahlhoefer, K. Schmidt-Hoberg, J. Kummer and S. Sarkar, *On the interpretation of dark matter self-interactions in abell 3827*, *Monthly Notices of the Royal Astronomical Society: Letters* **452** (jul, 2015) L54–L58.
- [54] H. M. Hodges, *Mirror baryons as the dark matter*, *Physical Review D* **47** (Jan, 1993) 456–459.
- [55] R. FOOT, *MIRROR MATTER-TYPE DARK MATTER*, *International Journal of Modern Physics D* **13** (Dec, 2004) 2161–2192.

- [56] D. E. Kaplan, G. Z. Krnjaic, K. R. Rehermann and C. M. Wells, *Atomic dark matter*, *Journal of Cosmology and Astroparticle Physics* **2010** (May, 2010) 021–021.
- [57] F.-Y. Cyr-Racine and K. Sigurdson, *Cosmology of atomic dark matter*, *Physical Review D* **87** (May, 2013) .
- [58] S. Davidson, S. Hannestad and G. Raffelt, *Updated bounds on milli-charged particles*, *Journal of High Energy Physics* **2000** (May, 2000) 003–003.
- [59] R. Foot, H. Lew and R. R. Volkas, *Electric-charge quantization*, *Journal of Physics G: Nuclear and Particle Physics* **19** (Mar, 1993) 361–372.
- [60] L. Chuzhoy and E. W. Kolb, *Reopening the window on charged dark matter*, *Journal of Cosmology and Astroparticle Physics* **2009** (Jul, 2009) 014–014.
- [61] S. D. McDermott, H.-B. Yu and K. M. Zurek, *Turning off the lights: How dark is dark matter?*, *Physical Review D* **83** (Mar, 2011) .
- [62] K. Kadota, T. Sekiguchi and H. Tashiro, *A new constraint on millicharged dark matter from galaxy clusters*, **1602.04009**.
- [63] P.-K. Hu, A. Kusenko and V. Takhistov, *Dark cosmic rays*, *Physics Letters B* **768** (May, 2017) 18–22.
- [64] D. Dunsky, L. J. Hall and K. Harigaya, *CHAMP cosmic rays*, *Journal of Cosmology and Astroparticle Physics* **2019** (Jul, 2019) 015–015.
- [65] M. D. Schwartz, *Quantum Field Theory and the Standard Model*. Cambridge University Press, 3, 2014.
- [66] J. A. Dror, R. Lasenby and M. Pospelov, *Dark forces coupled to nonconserved currents*, *Physical Review D* **96** (Oct, 2017) .
- [67] J. A. Dror, R. Lasenby and M. Pospelov, *New constraints on light vectors coupled to anomalous currents*, *Physical Review Letters* **119** (oct, 2017) .
- [68] J. A. Dror, *Discovering leptonic forces using nonconserved currents*, *Physical Review D* **101** (May, 2020) .
- [69] B. Holdom, *Two $U(1)$'s and ϵ charge shifts*, *Physics Letters B* **166** (Jan, 1986) 196–198.
- [70] R. Essig, J. A. Jaros, W. Wester, P. H. Adrian, S. Andreas, T. Averett et al., *Dark sectors and new, light, weakly-coupled particles*, *arxiv:1311.0029* (2013) .
- [71] S. Knapen, T. Lin and K. M. Zurek, *Light dark matter: Models and constraints*, *Physical Review D* **96** (Dec, 2017) .
- [72] A. S. GOLDHABER and M. M. NIETO, *Terrestrial and extraterrestrial limits on the photon mass*, *Reviews of Modern Physics* **43** (Jul, 1971) 277–296.
- [73] A. Caputo, H. Liu, S. Mishra-Sharma and J. T. Ruderman, *Dark photon oscillations in our inhomogeneous universe*, *arxiv:2002.05165* (2020) .
- [74] E. R. Williams, J. E. Faller and H. A. Hill, *New experimental test of coulomb's law: A laboratory upper limit on the photon rest mass*, *Physical Review Letters* **26** (Mar, 1971) 721–724.
- [75] D. F. Bartlett and S. Lögl, *Limits on an electromagnetic fifth force*, *Physical Review Letters* **61** (Nov, 1988) 2285–2287.

- [76] M. Betz, F. Caspers, M. Gasiior, M. Thumm and S. W. Rieger, *First results of the CERN resonant weakly interacting sub-eV particle search (CROWS)*, *Physical Review D* **88** (Oct, 2013) .
- [77] N. Vinyoles, A. Serenelli, F. Villante, S. Basu, J. Redondo and J. Isern, *New axion and hidden photon constraints from a solar data global fit*, *Journal of Cosmology and Astroparticle Physics* **2015** (Oct, 2015) 015–015.
- [78] L. D. Landau and E. M. Lifshitz, *Physical Kinetics*. 1981.
- [79] H. van Erkelens, *Relativistic boltzmann theory for a plasma*, *Physica A: Statistical Mechanics and its Applications* **107** (May, 1981) 48–70.
- [80] H. Vogel and J. Redondo, *Dark radiation constraints on minicharged particles in models with a hidden photon*, *Journal of Cosmology and Astroparticle Physics* **2014** (Feb, 2014) 029–029.
- [81] J. H. Chang, R. Essig and S. D. McDermott, *Supernova 1987a constraints on sub-GeV dark sectors, millicharged particles, the QCD axion, and an axion-like particle*, *Journal of High Energy Physics* **2018** (Sep, 2018) .
- [82] R. Essig, A. Manalaysay, J. Mardon, P. Sorensen and T. Volansky, *First direct detection limits on sub-GeV dark matter from XENON10*, *Physical Review Letters* **109** (Jul, 2012) .
- [83] R. Essig, T. Volansky and T.-T. Yu, *New constraints and prospects for sub-GeV dark matter scattering off electrons in xenon*, *Physical Review D* **96** (Aug, 2017) .
- [84] C. Dvorkin, T. Lin and K. Schutz, *Making dark matter out of light: Freeze-in from plasma effects*, *Physical Review D* **99** (Jun, 2019) .
- [85] R. Essig, J. Mardon and T. Volansky, *Direct detection of sub-GeV dark matter*, *Physical Review D* **85** (apr, 2012) .
- [86] M. Crisler, R. Essig, J. Estrada, G. Fernandez, J. Tiffenberg, M. S. Haro et al., *SENSEI: First direct-detection constraints on sub-GeV dark matter from a surface run*, *Physical Review Letters* **121** (Aug, 2018) .
- [87] O. Abramoff, L. Barak, I. M. Bloch, L. Chaplinsky, M. Crisler, Dawa et al., *SENSEI: Direct-detection constraints on sub-GeV dark matter from a shallow underground run using a prototype skipper CCD*, *Physical Review Letters* **122** (Apr, 2019) .
- [88] S. Knapen, T. Lin, M. Pyle and K. M. Zurek, *Detection of light dark matter with optical phonons in polar materials*, *Physics Letters B* **785** (Oct, 2018) 386–390.
- [89] S. Griffin, S. Knapen, T. Lin and K. M. Zurek, *Directional detection of light dark matter with polar materials*, *Physical Review D* **98** (Dec, 2018) .
- [90] A. Berlin, R. T. D’Agnolo, S. A. Ellis, P. Schuster and N. Toro, *Directly deflecting particle dark matter*, *Physical Review Letters* **124** (Jan, 2020) .
- [91] A. Caputo, L. Sberna, M. Frías, D. Blas, P. Pani, L. Shao et al., *Constraints on millicharged dark matter and axionlike particles from timing of radio waves*, *Physical Review D* **100** (sep, 2019) .
- [92] L. Hui, J. P. Ostriker, S. Tremaine and E. Witten, *Ultralight scalars as cosmological dark matter*, *Physical Review D* **95** (Feb, 2017) .
- [93] D. Levkov, A. Panin and I. Tkachev, *Gravitational bose-einstein condensation in the kinetic regime*, *Physical Review Letters* **121** (Oct, 2018) .

- [94] B. Bar-Or, J.-B. Fouvry and S. Tremaine, *Relaxation in a fuzzy dark matter halo*, *The Astrophysical Journal* **871** (Jan, 2019) 28.
- [95] J. J. Sakurai, *Modern Quantum Mechanics (Revised Edition)*. Addison Wesley, 1993.
- [96] D. V. Semikoz and I. I. Tkachev, *Kinetics of bose condensation*, *Physical Review Letters* **74** (Apr, 1995) 3093–3097.
- [97] P. Sikivie and Q. Yang, *Bose-einstein condensation of dark matter axions*, *Physical Review Letters* **103** (Sep, 2009) .
- [98] Y. Hochberg, M. Pyle, Y. Zhao and K. M. Zurek, *Detecting superlight dark matter with fermi-degenerate materials*, *Journal of High Energy Physics* **2016** (Aug, 2016) .
- [99] Y. Hochberg, Y. Kahn, M. Lisanti, C. G. Tully and K. M. Zurek, *Directional detection of dark matter with two-dimensional targets*, *Physics Letters B* **772** (Sep, 2017) 239–246.
- [100] Y. Hochberg, Y. Kahn, M. Lisanti, K. M. Zurek, A. G. Grushin, R. Ilan et al., *Detection of sub-MeV dark matter with three-dimensional dirac materials*, *Physical Review D* **97** (Jan, 2018) .
- [101] N. Craig, I. G. Garcia and S. Koren, *The weak scale from weak gravity*, *Journal of High Energy Physics* **2019** (Sep, 2019) .
- [102] M. Heikinheimo, M. Raidal, C. Spethmann and H. Veermae, *Collisionless shocks in self-interacting dark matter*, *Plasma Phys. Control. Fusion* **60** (2017) 014011, [1707.03662].
- [103] M. Abramowitz and I. A. Stegun, *Handbook of Mathematical Functions, With Formulas, Graphs, and Mathematical Tables*,. Dover Publications, Inc., USA, 1974.